

## Chapter 6

# Calcium Dynamics in Large Neuronal Models

ERIK DE SCHUTTER and PAUL SMOLEN

### 6.1 Introduction

Calcium is an important intracellular signaling molecule with rapid effect on the kinetics of many processes. As a consequence, almost all biophysically realistic models of neurons have to account for  $Ca^{2+}$  dynamics in some way, whether to model transmitter release or synaptic plasticity at individual synapses or to simulate the activation of  $K^+$  channels in a complete cell. While most neuronal models have only considered  $Ca^{2+}$  inflow through voltage or ligand-gated channels, release from intracellular  $Ca^{2+}$  stores may be physiologically as important.

This chapter continues to build on the basic approach to modeling ionic currents,  $Ca^{2+}$  diffusion, buffers and pumps introduced in Chapter 4 and assumes familiarity with those concepts. We describe how to simulate  $Ca^{2+}$  concentrations ( $[Ca^{2+}]$ ),  $Ca^{2+}$  release activated by  $Ca^{2+}$  itself or by inositol-1,4,5-triphosphate ( $IP_3$ ) and several other  $Ca^{2+}$  processes in complex models of dendritic trees (fig. 6.1). Whenever appropriate, we describe how we implemented the equations<sup>1</sup> in the GENESIS neural simulator as described in Chapter 12 (see also Bower and Beeman, 1995).

We are constructing biophysically realistic models of  $Ca^{2+}$  dynamics in the cerebellar Purkinje cell. A recent review of the biology of  $Ca^{2+}$  signaling in Purkinje cells can be found in Eilers, Plant and Konnerth (1996). Our models are used to investigate the dendritic physiology of these cells. An intriguing characteristic of the Purkinje cell is its very active dendrite, capable of generating large  $Ca^{2+}$  spikes (Llinás and Sugimori, 1980), combined with the tremendous

---

<sup>1</sup>For clarity we will use the same convention for the sign of membrane currents as used in Chapter 4, which is opposite to the convention used in GENESIS.

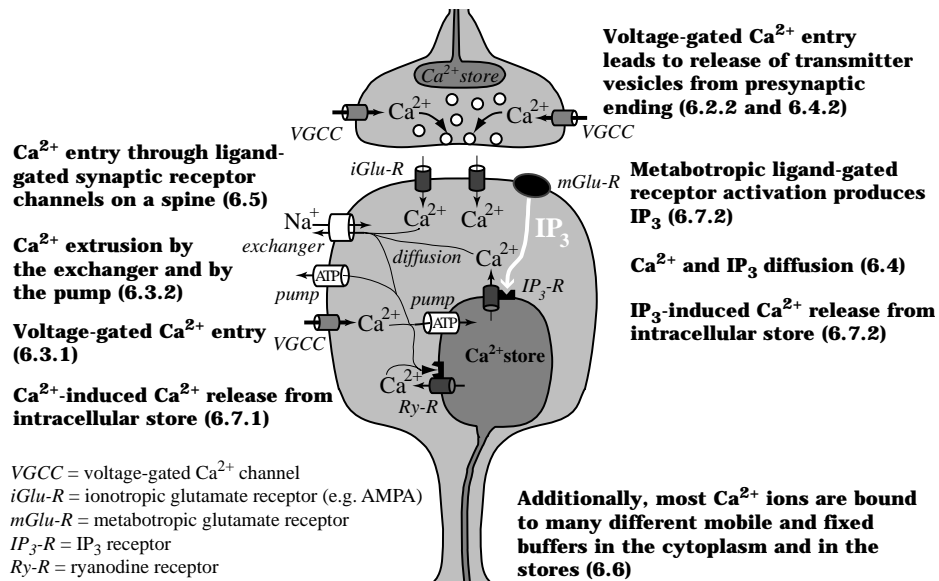


Figure 6.1: Overview of  $\text{Ca}^{2+}$  processes in a presynaptic ending and a dendritic spine. The bold text describes each process and points to the corresponding section in this chapter. Similar  $\text{Ca}^{2+}$  processes occur in the dendrite and soma.

synaptic convergence of over 150,000 excitatory parallel fiber synapses onto this dendrite (Harvey and Napper, 1991). In an earlier model of a rat Purkinje cell, we focused on accurately reproducing the properties of the different channel types, using Hodgkin-Huxley (1952) like equations (De Schutter and Bower, 1994a). One of those channels is the large conductance (BK or maxi-K)  $\text{Ca}^{2+}$ -activated  $\text{K}^+$  channel (Latorre et al., 1989). To model the activation of this channel  $[\text{Ca}^{2+}]$  had to be computed. At that time we choose to use a simple exponentially decaying  $\text{Ca}^{2+}$  pool (eq. 6.1), which is usually considered sufficient (e.g. Traub et al., 1991; Buchholtz et al., 1992; McCormick and Huguenard, 1992). A very important advantage of this approach was that only one parameter  $\beta$  needed to be defined for the entire model (eq. 6.1). In fact, when building a large active membrane model that includes  $\text{Ca}^{2+}$  dynamics, one is faced with a feedback loop: the  $\text{Ca}^{2+}$ -activated  $\text{K}^+$  channels hyperpolarize the membrane, leading to reduced  $\text{Ca}^{2+}$  influx. In other words, modifying the  $\text{Ca}^{2+}$  dynamics will alter  $\text{Ca}^{2+}$  influx, which is functionally equivalent to changing the maximum conductance levels ( $\bar{g}$ ) of the  $\text{Ca}^{2+}$  channels. Finding the appropriate  $\bar{g}$  levels for the channels at different locations in the model was difficult enough without the additional complications of simulating detailed  $\text{Ca}^{2+}$  dynamics. But even if  $[\text{Ca}^{2+}]$  is needed only to simulate the activation of  $\text{K}^+$  channels, the exponentially decaying pool model may not be sufficient. In fact, the slower activating small conductance (SK or AHP)  $\text{Ca}^{2+}$ -activated channel seems to sense different  $[\text{Ca}^{2+}]$  than the BK channel (Lancaster and Zucker, 1994) and

may even depend on  $Ca^{2+}$ -activated  $Ca^{2+}$  release (Sah, 1996). Multiple types of  $Ca^{2+}$ -activated  $K^+$  channels are present in Purkinje cells (Gruol, Jacquin and Yool, 1991), but kinetic data on their  $Ca^{2+}$  dependence are lacking.

Our earlier version of the Purkinje cell model was quite successful in reproducing synaptic responses (De Schutter and Bower, 1994b). It predicted that a small, localized parallel fiber input could cause a focal activation of dendritic  $Ca^{2+}$  channels (De Schutter and Bower, 1994c), which was later confirmed experimentally (Eilers, Augustine and Konnerth, 1995). This dendritic  $Ca^{2+}$  channel activation amplifies parallel fiber evoked EPSPs, making the somatic response of the Purkinje cell model insensitive to the location of its parallel fiber inputs. This is in direct contrast to the predictions from passive membrane modeling (Chapter 2). Even more interesting is that the active dendrite amplifies subthreshold background synaptic inputs also, resulting in an increased variability of the somatic response to synchronous parallel fiber input (De Schutter, 1995). This turns out to be caused by the  $Ca^{2+}$ -activated  $K^+$  channels and raises the question of whether other mechanisms influencing dendritic [ $Ca^{2+}$ ] could modify synaptic responses too.

It has been known for a long time that Purkinje cell dendrites contain high densities of intracellular  $Ca^{2+}$  stores (Martone et al., 1993), making these cells a popular preparation for the study of  $Ca^{2+}$  release mechanisms (Berridge, 1993). Calcium release from these stores can be activated both by synaptic stimulation of metabotropic glutamate receptors (Llano et al., 1991) and by  $Ca^{2+}$  itself (Llano, DiPolo and Marty, 1994; Kano et al., 1995). But the physiological role of these processes remains unclear and positive evidence for  $Ca^{2+}$  release under normal *in vivo* conditions is still lacking. It is unlikely that this question will be experimentally resolved soon, as the present recording techniques are not sensitive enough. We will discuss in section 6.6.4 the limitations of fluorescent  $Ca^{2+}$  indicators. Another problem experimentalists face is the lack of a fast ‘calcium clamp’, similar to the voltage clamp procedure. As a consequence, the kinetics of many  $Ca^{2+}$  related procedures have been studied under steady state conditions exclusively and only a few gating studies of  $Ca^{2+}$ -activated  $K^+$  channels are available (e.g. Moczydlowski and Latorre, 1983). The introduction of caged release of  $Ca^{2+}$  or of second messengers (Wang and Augustine, 1995) has allowed more detailed kinetic studies (Györke and Fill, 1993).

These experimental limitations make developing realistic models of  $Ca^{2+}$  dynamics in Purkinje cells more important and more difficult at the same time. We and others have demonstrated that compartmental models of neurons incorporating Hodgkin-Huxley like channels can be used to probe single cell function *in vivo* (Bernander et al., 1991; De Schutter and Bower, 1994b). This is important as, in the case of the Purkinje cell, even simple experiments demonstrate that the firing properties *in vivo* are completely different from those in slice (Jaeger, De Schutter and Bower, 1997). Similarly, we expect our modeling to contribute to a better understanding of the role of intracellular  $Ca^{2+}$  release *in vivo* and of the importance of  $Ca^{2+}$  channels on spines (Denk, Sugimori and Llinás, 1995).

In this chapter we will describe the methods we have used to develop a more

detailed model of the  $Ca^{2+}$  dynamics in the Purkinje cell and present some preliminary results to demonstrate the importance of simulating these mechanisms. We will not restrict ourselves to describing this model exclusively, but instead also consider other methods relevant to the modeling of ionic concentrations. In fact, we start by considering models which are not realistic at all.

## 6.2 Phenomenological Models of Calcium Dynamics

The first question that should always be asked is if it is necessary to simulate  $Ca^{2+}$  dynamics with a complete biophysical model including  $Ca^{2+}$  diffusion, buffers and pumps. If the only reason to simulate  $[Ca^{2+}]$  is to couple two processes which are of interest to the modeler, it might be better to use a simple *ad hoc* model that computes an ‘effective  $[Ca^{2+}]$ ’. Such a ‘phenomenological’ model will contain less parameters than a biophysical model and will therefore be much easier to constrain with experimental data. Especially if the relevant  $Ca^{2+}$  concentrations have never been measured a biophysical model of  $[Ca^{2+}]$  may *look* realistic, while it has in effect little resemblance to the real system.

### 6.2.1 The simple pool model of calcium concentration

The exponentially decaying  $Ca^{2+}$  pool (Traub and Llinás, 1977) is the most frequently used model of  $[Ca^{2+}]$  in neuronal simulations. It describes the change in  $[Ca^{2+}]$  in a single compartment as:

$$\frac{d[Ca^{2+}]}{dt} = -\frac{I_{Ca}}{2Fv} - \beta ([Ca^{2+}] - [Ca^{2+}]_{min}) \quad (6.1)$$

The first term of this equation describes the change caused by  $Ca^{2+}$  inflow into a compartment with volume  $v$  ( $F$  is Faraday’s constant, see eq. 4.15), the second term is a decay term which causes  $[Ca^{2+}]$  to relax exponentially with a time constant  $1/\beta$  to the baseline concentration  $[Ca^{2+}]_{min}$ . The constant  $\beta$  lumps together many different mechanisms causing a reduction in  $[Ca^{2+}]$ , and is often referred to as a diffusion rate constant (McCormick and Huguenard, 1992) or a  $Ca^{2+}$  buffering constant (LeMasson, Marder and Abbott, 1993).

The implicit formulation of eq. 6.1 used in the GENESIS neural simulator is based on the trapezoidal rule and depends on the computation of  $I_{Ca}$  at a time offset by half a time-step  $\Delta t$  from the time at which voltage is computed (see section 14.3.6):

$$\begin{aligned} [Ca^{2+}]_{t+\Delta t} = & [Ca^{2+}]_{min} + \frac{([Ca^{2+}]_t - [Ca^{2+}]_{min}) (1 - \beta \frac{\Delta t}{2})}{1 + \beta \frac{\Delta t}{2}} \\ & - \frac{\Delta t}{1 + \beta \frac{\Delta t}{2}} \frac{I_{Ca,t+\Delta t/2}}{2Fv} \end{aligned} \quad (6.2)$$

Values for  $\beta$  range from  $0.02 \text{ msec}^{-1}$  (Traub and Llinás, 1977) to  $10 \text{ msec}^{-1}$  (De Schutter and Bower, 1994a). A large  $\beta$  makes  $[Ca^{2+}]$  follow changes in  $I_{Ca}$  closely with minimal accumulation of  $Ca^{2+}$ . An often used modification to eq. 6.1 is to not compute inflow into the complete compartment, but instead restrict  $v$  to the volume of a submembrane shell (Traub et al., 1991; De Schutter and Bower, 1994a).

Eq. 6.1 is useful for neuronal models where  $[Ca^{2+}]$  is needed only to simulate the activation of the large conductance (BK)  $Ca^{2+}$ -activated  $K^+$  channel (Latorre et al., 1989). But it can also be used in more complex models that include  $Ca^{2+}$ -regulated molecular processes. A nice example is the activity-dependent regulation of channel densities in a model by LeMasson, Marder and Abbott (1993). The  $[Ca^{2+}]$  was computed by eq. 6.1 and then used to dynamically change the densities ( $\bar{g}$ ) of all the ionic channels represented in the model:

$$\tau \frac{d\bar{g}}{dt} = \frac{G_T}{1 + e^{\gamma([Ca^{2+}] - C_T)}} - \bar{g} \quad (6.3)$$

In eq. 6.3 a rise of  $[Ca^{2+}]$  above  $C_T$  will cause a slow increase of the maximum conductance  $\bar{g}$  for  $K^+$  channels ( $\gamma < 0$ ) and a reduction for the conductance of  $Ca^{2+}$  and  $Na^+$  channels ( $\gamma > 0$ ). The authors showed that, depending on the target concentration  $C_T$  and the maximum conductance  $G_T$ , the conductance levels in single compartment models change dynamically till the modeled cell becomes silent, regularly firing or bursting. Later the same method was applied successfully to a multi-compartmental model of a pyramidal neuron (Siegel, Marder and Abbott, 1994). These results demonstrate how one can combine biophysically realistic models (Hodgkin-Huxley like equations) with an extremely simple *ad hoc* model to simulate complex dynamic processes.

### 6.2.2 A Model of Synaptic Transmitter Release

If the exponentially decaying pool of eq. 6.1 is not sufficient to model the dynamics of the system, it might still be appropriate to use an *ad hoc* model with its parameters directly fitted to the available physiological data. Such *ad hoc* models can replicate the desired behavior to a high degree of accuracy. This approach was used in a model of graded synaptic transmission between leech neurons (De Schutter, Angstadt and Calabrese, 1993). In this case our goal was to study the role of graded synaptic inhibition in the generation of oscillatory network activity (Calabrese and De Schutter, 1992). The actual mechanisms controlling transmitter release were not relevant to this question, but the model needed to replicate the relation between presynaptic voltage ( $V_{pre}$ ) and postsynaptic current ( $I_{syn}$ ) accurately. As voltage-gated  $Ca^{2+}$  inflow is responsible for spike-mediated synaptic transmission (Augustine, Charlton and Smith, 1985; Parnas, Parnas and Hochner, 1991), it seemed evident to postulate a similar mechanism for graded release. Extensive experimental data were available, consisting of dual voltage clamps of coupled interneurons which simultaneously measured the  $Ca^{2+}$  currents ( $I_{Ca}$ ) in the presynaptic cell and the synaptic current ( $I_{syn}$ ) in the postsynaptic cell (Angstadt and Calabrese, 1991). We decided

to build an *ad hoc* model relating these two variables:

$$\frac{d[P_{pre}]}{dt} = \max(-I_{Ca} - A(V_{pre}), 0) - B(V_{pre})[P_{pre}] \quad (6.4)$$

$$I_{syn} = \bar{g}[P_{pre}]^3(V_{post} - E_{syn}) \quad (6.5)$$

These equations relate an effective  $Ca^{2+}$  concentration  $[P_{pre}]$  to the voltage-gated  $Ca^{2+}$  inflow  $I_{Ca}$  (eq. 6.4), with transmitter release and the postsynaptic conductance proportional to the third power of  $[P_{pre}]$  (Augustine, Charlton and Smith, 1985; eq. 6.5). The  $Ca^{2+}$  currents were described by conventional Hodgkin-Huxley like equations. A first version of the *ad hoc* model contained only the  $Ca^{2+}$  inflow  $I_{Ca}$  and the removal factor  $B$  (similar to  $\beta$  in eq. 6.1 with  $[Ca^{2+}]_{min} = 0$ ), but such a model could not adequately fit the data. A transient  $I_{Ca}$  is activated at the beginning of each depolarizing voltage-step, causing the initial  $Ca^{2+}$  inflow to be much larger than  $I_{syn}$ . Therefore a parameter  $A$  which subtracts the part of the  $Ca^{2+}$  current that is ineffective in causing transmitter release was introduced in eq. 6.4. All that remained to be done, was to find voltage-dependent equations for the parameters  $A$  and  $B$  by fitting the model to each of the six voltage-steps (De Schutter, Angstadt and Calabrese, 1993).

This simple model of computing an ‘effective  $Ca^{2+}$  concentration’  $[P_{pre}]$  from the  $Ca^{2+}$  inflow, was highly effective in reproducing the oscillatory firing behavior of two reciprocally coupled interneurons (Calabrese and De Schutter, 1992; De Schutter, Angstadt and Calabrese, 1993). Subsequently, the model was further improved by making the dependence on  $[P_{pre}]$  in eq 6.5 saturating (Nadim et al., 1995) which allowed several model predictions to be confirmed experimentally (Olsen and Calabrese, 1996).

This example demonstrates the advantages and disadvantages of such phenomenological models. The model was quite effective in the network simulations for which it was built. It computed fast and it was robust for large variations of other parameters in the model (Nadim et al., 1995). Yet it also required specific modifications to the simulator code before it could be used. Most general neural simulators (De Schutter, 1992) will require at least a recompilation and often also modifications of the source code before they can run an *ad hoc* model.

Another consequence of this approach is that the properties of the model will reflect the kind of data that were used to generate it. In this specific example, both the parameters  $A$  and  $B$  are voltage-dependent. This was an artifact caused by the use of voltage-clamp data, where the membrane potential is of course accurately known. While there is some evidence for the involvement of voltage-dependent processes in transmitter vesicle docking mechanisms (Parnas, Parnas and Hochner, 1991), it should be emphasized that the voltage-dependence of the parameters in eq. 6.4 has no biophysical meaning. In practice, however, the relevance of such models may be unclear unless it is made very plain which parts are biophysically realistic (the Hodgkin-Huxley equations) and which are not (e.g. eq. 6.4).

### 6.3 Rectifying Calcium Channels and Pumps

In this section we describe methods to model non-ohmic currents and the electrogenic effect of pumps. The simulation of ohmic currents, i.e. currents with a linear dependence on voltage, has been described in Chapter 4.

We will also start describing the results obtained with the new Purkinje cell model. More detailed information on this model, the parameter values used, and how to obtain the GENESIS scripts to run it can be found in Appendix A.

#### 6.3.1 Goldman-Hodgkin-Katz equation

The standard model of ionic currents introduced by Hodgkin and Huxley (1952) is ohmic, i.e. it assumes that the instantaneous current-voltage relation is linear. This is not true if the external concentration of the permeant ion is very different from the internal one, causing current to pass more easily in one direction (rectification; Hille 1991). Calcium ions have a concentration ratio of about 50,000:1, which makes outward  $Ca^{2+}$  currents very small. The concentration dependent rectification of ionic currents is usually described by the constant field equation, commonly called the GHK equation (Goldman, 1943; Hodgkin and Katz, 1949):

$$I_{Ca} = P_{Ca} z_{Ca}^2 \frac{VF^2}{RT} \frac{[Ca^{2+}]_i - [Ca^{2+}]_o e^{-z_{Ca}FV/RT}}{1 - e^{-z_{Ca}FV/RT}} \quad (6.6)$$

with  $P_{Ca}$  as the channel permeability to  $Ca^{2+}$  ions,  $z_{Ca}$  the valency (here equal to +2),  $V$  the voltage and  $R$ ,  $F$  and  $T$  the gas constant, Faraday constant and absolute temperature respectively. The assumptions underlying this equation can be found in Jack, Noble and Tsien (1975) and in Hille (1991). When the GHK equation is used,  $Ca^{2+}$  currents become quite non-linear and small above 0 mV, but they will still reverse above +120 mV, i.e. at the Nernst potential for  $Ca^{2+}$ . To obtain the reversal potential of between +40 and +70 mV that is observed experimentally, a second GHK equation must be included to model the permeability of the  $Ca^{2+}$  channel to  $K^+$  ions (Hille, 1991).

To use eq. 6.6 in standard compartmental models the voltage-dependent gating of  $I_{Ca}$  needs to be incorporated. Strictly speaking the gating concept is incompatible with the GHK equation because the latter does not consider membrane pores at all (Hille, 1991)! The permeability  $P_{Ca}$  is in fact a measure of how easily  $Ca^{2+}$  ions diffuse across the cell membrane (units  $m/sec$ ) and is usually expressed relative to other permeabilities, e.g.  $P_{Ca}/P_{Na}$  is the relative permeability of a  $Na^+$  channel to  $Ca^{2+}$  ions. In practice, however, Hodgkin-Huxley-like equations can be used to compute  $m_{Ca}$  and  $h_{Ca}$  (see Chapter 4) and from these the voltage-dependent membrane permeability to  $Ca^{2+}$  as:

$$P_{Ca}(V) = \bar{g} m_{Ca}^2 h_{Ca} \quad (6.7)$$

Note that in this approximation  $\bar{g}$  has the dimensions of a permeability ( $m/sec$ ) and should be about  $10^7$  times smaller than the corresponding maximum conductance  $\bar{g}$  (in *Siemens*, eq. 4.5) to obtain a similar amplitude  $I_{Ca}$ .

Once  $P_{Ca}$  is computed, it is trivial to use eq. 6.6 to replace the ohmic equation for  $I_{Ca}$  in the voltage equation if a forward Euler method is used (eq. 14.46). But how should one incorporate eq. 6.6 into an implicit method (e.g. eq. 14.47)? One solution is to accept that the GHK equation makes the voltage equation non-linear and use iterative solution methods (Chapter 14). We have implemented a faster, but potentially less accurate method in the GENESIS simulator. This method uses a local linearization of the GHK equation. In addition to eq. 6.6 its derivative over  $V$ , the slope conductance (Jack, Noble and Tsien, 1975), is also computed:

$$\begin{aligned} g'_{Ca} &= \frac{dI_{Ca}}{dV} \\ &= P_{Ca} z_{Ca}^2 \frac{F^2}{RT} \frac{[Ca^{2+}]_i - [Ca^{2+}]_o e^{-z_{Ca}FV/RT}}{1 - e^{-z_{Ca}FV/RT}} \\ &\quad - P_{Ca} z_{Ca}^3 \frac{F^3}{R^2 T^2} ([Ca^{2+}]_i - [Ca^{2+}]_o) \frac{V e^{-z_{Ca}FV/RT}}{(1 - e^{-z_{Ca}FV/RT})^2} \end{aligned} \quad (6.8)$$

Assuming that  $I_{Ca}$  is linear for  $V$  over the step  $\Delta t$ , the slope conductance  $g'_{Ca}$  can be used to compute a ‘slope reversal potential’:

$$E'_{Ca} = \frac{g'_{Ca} V - I_{Ca}}{g'_{Ca}} \quad (6.9)$$

As long as  $g'_{Ca}$  is positive it can be used together with  $E'_{Ca}$  in eq. 14.47. This solution was perfectly stable and fast for the computation of the two  $Ca^{2+}$  currents in the Purkinje cell model. The local linearization approach of eqs. 6.8–6.9 works because the GHK current deviates most from linearity when it is small (Hille 1991, p. 343).

### 6.3.2 Calcium pumps

Other types of non-ohmic currents which are included in the Purkinje cell model are membrane pumps. Usually the electrogenic component of such pumps is neglected (e.g. Chapter 4), but we will demonstrate that these pumps can carry a sizable current. As described in section 4.6.4, two major types of plasma membrane  $Ca^{2+}$ -pumping mechanisms have been identified. The  $Ca^{2+} - ATPase$  is a high affinity, low capacity pump causing an outward current. Its  $Ca^{2+}$  dependence can be approximated with a Hill function (Garrahan and Rega, 1990; Zador, Koch and Brown, 1990):

$$I_{Ca-ATP} = z_{Ca} F a_i V_{max} \frac{[Ca^{2+}]_i}{K_d + [Ca^{2+}]_i} \quad (6.10)$$

where  $V_{max}$  is the maximal pump rate (units of  $mol\ cm^{-2}\ ms^{-1}$ , taking into account the surface density of the pump),  $K_d$  the dissociation constant and  $a_i$  the outer membrane surface area of the compartment. Eq. 4.15 can be used to compute the decrease in  $[Ca^{2+}]_i$  caused by the pump. Because eq. 6.10 has no voltage dependence, it can be considered constant during the step  $\Delta t$  in the

voltage equation. Consequently, it can be divided by the membrane capacitance  $C_m$  and added as  $\frac{A_i}{C_m} I_{Ca-ATP}$  to the right sides of eq. 14.46 or 14.47.

**$Na^+$ - $Ca^{2+}$  exchanger** The second pump is the  $Na^+$ - $Ca^{2+}$  exchanger which has a lower affinity for  $Ca^{2+}$ , but a higher capacity to remove  $Ca^{2+}$ . It uses the transmembrane  $Na^+$  gradient to move  $Ca^{2+}$  ions, with a stoichiometry of 3:1. DiFrancesco and Noble (1985) have developed a model of the cardiac  $Na^+$ - $Ca^{2+}$  exchanger, which has been applied to neuronal models (Gabbiani, Midtgaard and Knöpfel, 1994):

$$I_{NaCa} = k_{NaCa} a_i \left( [Ca^{2+}]_o [Na^+]_i^3 e^{\gamma FV/RT} - [Ca^{2+}]_i [Na^+]_o^3 e^{(\gamma-1)FV/RT} \right) \quad (6.11)$$

with  $k_{NaCa}$  (units of  $\mu A mM^{-4} cm^{-2}$ ) as a factor controlling the maximum exchange current and  $\gamma$  a partition parameter representing the fractional position within the membrane of the voltage-sensitive energy barrier (usually taken to be 0.38; Hille, 1991). If  $[Ca^{2+}]_i$  is sufficiently high eq. 6.11 results in an inward current. Eq. 4.15 with a net ‘effective valency’  $z$  of  $-1$  can be used to compute the change of  $[Ca^{2+}]_i$ . This current is, like the GHK current, voltage-dependent and non-ohmic. To solve it implicitly, we have used a similar approach by computing a slope conductance  $g'$  and using eq. 6.9 to compute the ‘slope reversal potential’. Unfortunately, the dependence of the  $Na^+$ - $Ca^{2+}$  exchange current on voltage becomes less linear when  $I_{NaCa}$  increases due to a rise in  $[Ca^{2+}]_i$ , but as it remains a small current (fig. 6.2) the inaccuracies introduced by the local linearization are small.

**Purkinje cell model** The  $Ca^{2+} - ATPase$  pump was modeled using eq. 6.10 with a  $V_{max}$  of  $9 \cdot 10^{-11} mol cm^{-2} ms^{-1}$  and a  $K_d$  of  $1 \mu M$ . The  $Na^+$ - $Ca^{2+}$  exchanger had a  $k_{NaCa}$  of  $1.4 \cdot 10^{-3} \mu A mM^{-4} cm^{-2}$  (eq. 6.11).  $Na^+$  concentrations were assumed to be constant at  $10 mM$  inside and  $125 mM$  outside (Aidley, 1989).

Fig. 6.2 compares the electrogenic currents to the voltage-gated currents during dendritic  $Ca^{2+}$  spikes. As expected from their stoichiometry, the pump caused an outward current and the exchanger an inward one. In between dendritic spikes the high-affinity pump dominated, contributing significantly to the total outward current of the model. During the dendritic spike the exchanger partially counteracted the pump current, but not completely. This is because the depolarization diminished the exchange current, without affecting the  $Ca^{2+} - ATPase$  pump. The relative contributions of both depended, however, on the exact maximum pump rates  $V_{max}$  and  $k_{NaCa}$  used, parameters for which unfortunately little data are available.

The electrogenic current of the pump and exchanger contributed significantly to the resting membrane potential ( $-68 mV$  in the model, with a resting  $[Ca^{2+}]$  of  $40 nM$ ). At rest the outward pump current ( $-0.81 pA$  in the compartment shown in fig. 6.2) counteracted the small inward  $I_{Ca}$  currents ( $0.92 pA$ ). At

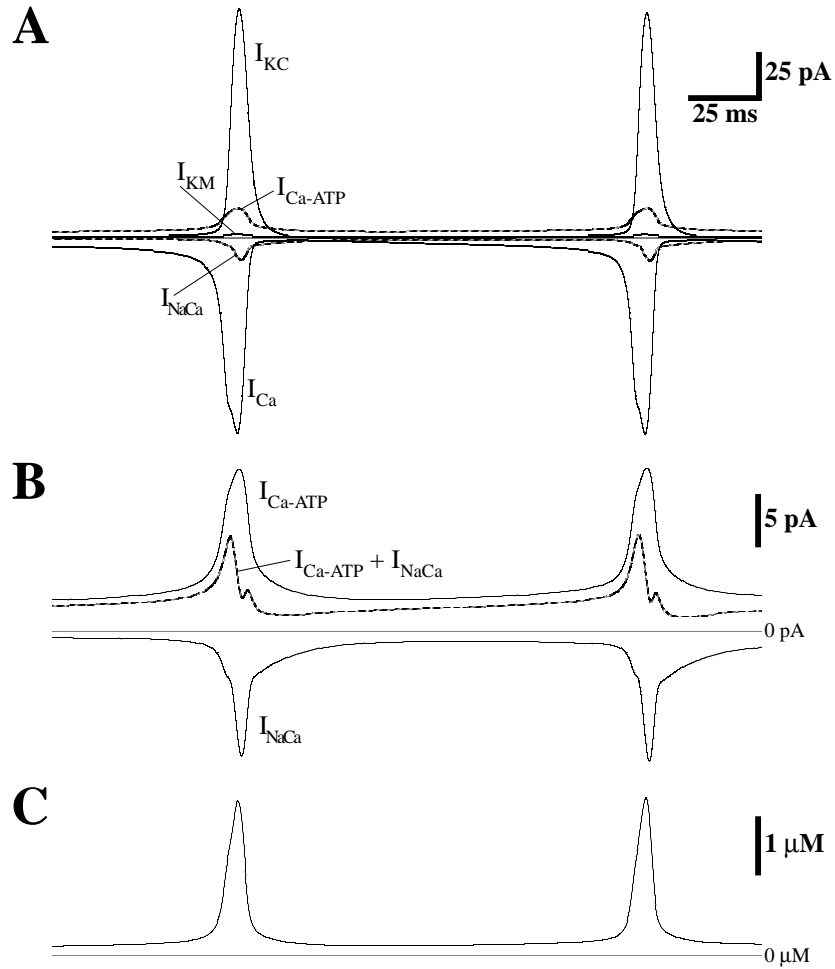


Figure 6.2: Voltage and  $Ca^{2+}$ -gated currents in a spiny dendritic compartment during two  $Ca^{2+}$  spikes in the Purkinje cell model. **A.** Comparison of the electrogenic  $Ca^{2+} - ATPase$  pump and  $Na^+ - Ca^{2+}$  exchanger currents (broken lines) with the  $Ca^{2+}$  and  $K^+$  currents (full lines). The persistent outward  $Ca^{2+} - ATPase$  pump current is the largest dendritic current in between the two spikes. **B.** The two electrogenic currents and their sum (broken line) are shown at a larger scale. **C.**  $[Ca^{2+}]$  in the submembrane shell of the same spiny dendritic compartment.

rest the  $Na^+$ - $Ca^{2+}$  exchanger was also *outward* ( $-0.27$  pA), but its size depended critically on the resting  $[Na^+]_i$ . Outward exchanger currents have been described in the experimental literature (Reeves, 1990).

**Tabulated equations** Solving eq. 6.6 and eqs. 6.8–6.9 (or eq. 6.11) requires many computations. Therefore, the GENESIS neural simulator uses precomputed tables whenever possible. If  $[Ca^{2+}]_o$ ,  $[Na^+]_i$  and  $[Na^+]_o$  are constant, a two-dimensional table indexed by  $V$  and  $[Ca^{2+}]_i$  can be precomputed to rapidly obtain the slope conductance and reversal potential.

It is always difficult to predict if the use of precomputed tables will increase simulation speed or not. Two factors determine the speed of tabulated functions: memory access, which tends to be slower than floating point operations on modern computers, and interpolation. Interpolation may not be necessary for purely voltage-dependent functions (Chapter 14). But with  $Ca^{2+}$ -dependent functions it is difficult to make the table increment sufficiently small, because the table must include a range covering several orders of magnitude. Also, in the case of two-dimensional tables memory limitations simply do not allow the use of small table increments. Even if they are not faster, tables do have the advantage of allowing many different functions to be implemented by the same code. Moreover, if tables are used, one does not have to check continuously for singularities (e.g.  $V = 0$  in the denominator of eqs. 6.6 and 6.8). Therefore, the implicit methods in GENESIS 2.1 make extensive use of interpolated tables.

## 6.4 Diffusion of Calcium

In this section we extend the solution for buffered diffusion in a single spherical compartment, which was introduced in Chapter 4, to diffusion in large neuronal models with several compartments having different geometries. A compartment is considered to be isopotential (Chapter 3), but because of the short space constant of diffusion (section 6.6.5) it cannot be isoconcentration. In a complete biophysical representation the coupling between compartments occurs both by potential and by concentration. The former has been described in detail in Chapters 2 and 3 as the axial current flow between compartments, here we consider only diffusion. In general, diffusion of  $Ca^{2+}$  and other molecules needs to be treated in three dimensions (see also section 6.4.2). But, if  $Ca^{2+}$  fluxes are assumed to be uniform across the membrane of a cylindrical compartment, no longitudinal gradients will be created within the compartment. As a consequence, only radial diffusion needs to be considered within compartments, allowing the three-dimensional diffusion system to be reduced to a much easier to compute one-dimensional system. Such a one-dimensional approach neglects of course the concentration gradients between compartments, which should cause longitudinal fluxes. In practice, however, concentration gradients between compartments (at similar depths) are much smaller than the radial gradients within compartments (compare Plate .8D to fig. 6.6A).

### 6.4.1 One-dimensional diffusion in cylinders and spheres

Fick's first law (Fick, 1855) states that the diffusion flux  $J_{Ca,D}$  is proportional and opposite to the concentration gradient:

$$J_{Ca,D} = -a D_{Ca} \frac{\partial [Ca^{2+}]}{\partial x} \quad (6.12)$$

where the one-dimensional flux  $J_{Ca,D}$  has the units of *mol/sec*,  $a$  is the area across which diffusion occurs and  $D_{Ca}$  is the diffusion constant for  $Ca^{2+}$ . Discretization of eq. 6.12 leads to:

$$J_{i \rightarrow j} = D_{Ca} \frac{a_{i,j}}{\delta_{i,j}} ([Ca^{2+}]_i - [Ca^{2+}]_j) \quad (6.13)$$

with  $\delta_{i,j}$  as the distance between the points where  $[Ca^{2+}]_i$  and  $[Ca^{2+}]_j$  are measured. The change in  $[Ca^{2+}]$  caused by the diffusion flux  $J_{i \rightarrow j}$  will be determined by the volume  $v$  in which  $J_{i \rightarrow j}$  is diluted. This leads to the explicit forward Euler formulation for the change in  $[Ca^{2+}]_i$  due to one-dimensional diffusion between the shells  $i$  and  $i+1$ :

$$[Ca^{2+}]_{i,t+\Delta t} - [Ca^{2+}]_{i,t} = \Delta t D_{Ca} C_{i,i+1} ([Ca^{2+}]_{i+1,t} - [Ca^{2+}]_{i,t}) \quad (6.14)$$

where the coupling constant  $C_{i,i+1}$  is defined as:

$$C_{i,i+1} = \frac{a_{i,i+1}}{v_i \delta_{i,i+1}} \quad (6.15)$$

This coupling constant (units  $1/m^2$ ) depends on the specific geometry of the shells and will usually be different for any pair of neighboring shells. The implicit Crank-Nicholson formulation of eq. 6.14 is:

$$\begin{aligned} [Ca^{2+}]_{i,t+\Delta t} - [Ca^{2+}]_{i,t} = \\ \frac{\Delta t}{2} D_{Ca} C_{i,i+1} \left( [Ca^{2+}]_{i+1,t+\Delta t} - [Ca^{2+}]_{i,t+\Delta t} \right. \\ \left. + [Ca^{2+}]_{i+1,t} - [Ca^{2+}]_{i,t} \right) \end{aligned} \quad (6.16)$$

The Crank-Nicolson method is the preferred method for the solution of diffusion problems (Fletcher, 1991; Press et al., 1992). Usually, a shell  $i-1$  will also be present. This gives rise to a second set of terms in eq. 6.14 and 6.16. For eq. 6.16, adding these terms and rewriting gives:

$$\begin{aligned} & -\frac{\Delta t}{2} D_{Ca} C_{i-1,i} [Ca^{2+}]_{i-1,t+\Delta t} \\ & + \left( 1 + \frac{\Delta t}{2} D_{Ca} (C_{i-1,i} + C_{i,i+1}) \right) [Ca^{2+}]_{i,t+\Delta t} \\ & - \frac{\Delta t}{2} D_{Ca} C_{i,i+1} [Ca^{2+}]_{i+1,t+\Delta t} \\ = & \frac{\Delta t}{2} D_{Ca} C_{i-1,i} [Ca^{2+}]_{i-1,t} + \left( 1 - \frac{\Delta t}{2} D_{Ca} (C_{i-1,i} + C_{i,i+1}) \right) [Ca^{2+}]_{i,t} \\ & + \frac{\Delta t}{2} D_{Ca} C_{i,i+1} [Ca^{2+}]_{i+1,t} + \frac{\Delta t}{2} \frac{J_{i,t+\Delta t/2}}{v_i} \end{aligned} \quad (6.17)$$

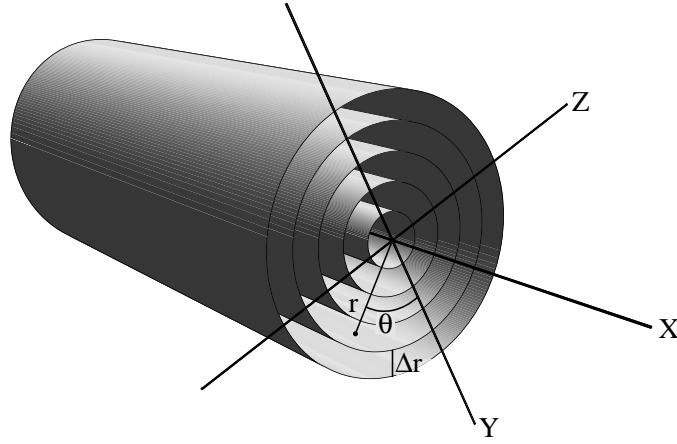


Figure 6.3: Comparison of Cartesian coordinates  $(x, y, z)$  and cylindrical ones  $(r, \theta, x)$ . To simulate radial one-dimensional diffusion the cylindrical volume is discretized into a number of shells each with a thickness  $\Delta r$ . While comparing with experimental data,  $[Ca^{2+}]_{i,t}$  should be taken as the concentration in the center of shell  $i$ .

where we have added an unspecified flux  $J_i$ , which could be the transmembrane  $Ca^{2+}$  inflow into the volume  $v_i$  of shell  $i$  (see eq. 4.15) or the flux from an intracellular store (section 6.7.3). The system of equations described by eq. 6.17 can be solved very efficiently because its corresponding matrix is tridiagonal with diagonal dominance (see section 14.3.4; Press et al., 1992). The Crank-Nicholson method is second order accurate in both space and time, but since the diffusion equation is a parabolic equation its accuracy depends completely on how exactly the boundary conditions are solved (Fletcher, 1991). In most neuronal models the most important boundary condition is the transmembrane flux  $J_i$ , which should be computed at the same  $\Delta t$  as eq. 6.17.

**Compartmental models of neurons** Electrical compartments usually represent cylinders so it is convenient to use similar geometries and cylindrical coordinates for the simulation of diffusion (fig. 6.3).

For radial diffusion into a cylinder the coupling constant (eq. 6.15) becomes:

$$C_{i,i+1} = \frac{2(i+1)}{(2i+1)\Delta r^2} \quad (6.18)$$

and for a sphere:

$$C_{i,i+1} = \frac{3(i+1)^2}{(3i^2 + 3i + 1)\Delta r^2} \quad (6.19)$$

where  $\Delta r$  is the thickness of the shells (fig. 6.3) and  $i = 0$  is the central shell. The diameter of the electrical compartment should be  $d = 2 \cdot n\Delta r$ .

Equations 6.18–6.19 assume that all shells in a compartment have the same thickness  $\Delta r$ . This assumption may not be practical to enforce in a multi-compartmental model based on a reconstructed morphology. Because of the variability in compartmental diameters, this would require different values for  $\Delta r$  in each compartment. This is not a good solution because with each compartment having a different thickness  $\Delta r$  for the outer submembrane shell, the computed  $[Ca^{2+}]$  will vary between compartments even if the activation of  $Ca^{2+}$  channels is identical. This not only complicates comparisons between  $[Ca^{2+}]$  of different compartments, but also leads to unphysiological differences in the activation of  $Ca^{2+}$ -activated  $K^+$  channels.

It is better to use the same value for  $\Delta r$  throughout the model, which has two consequences. First, the number of shells in a compartment is not constant. This is beneficial as it keeps the spatial resolution of the diffusion equations constant. Second, the radius of any given compartment is usually not an integral multiple of  $\Delta r$ . In that case, one shell must have a different  $\Delta r$  and for the reasons outlined in the previous paragraph this cannot be the submembrane shell. The best choice is the central shell  $i = 0$  and eq. 6.15 can be used to compute  $C_{0,1}$ , with  $\delta_{0,1} = \Delta r_0 + \Delta r_1/2$ . It is important to realize that eqs. 6.14 and 6.16 become unstable if the geometry is very asymmetric. For example, if  $\Delta r_i$  is much smaller than  $\Delta r_{i+1}$ , a small  $\Delta t$  will be needed for correct convergence. In practice, this means that  $\Delta r_0$  should not be too small. In the GENESIS neural simulator a thin central shell is created only if  $\Delta r_0 > \Delta r/4$ , otherwise the central shell has a thickness of  $\Delta r$  plus the small remainder.

Carnevale and Rosenthal (1992) discuss the relation between  $\Delta r$  and the temporal accuracy of the discretized solution. In general this accuracy will be poor in the submillisecond range for extremely fast changes in concentration, which are fortunately rare in biological simulations. Note that if  $[Ca^{2+}]_{i,t}$  is used to compute the activation of  $Ca^{2+}$ -activated  $K^+$  channels a change of  $\Delta r$  throughout the model will always vary the fine details of the computed spiking pattern. In a typical neuronal model one cannot expect the solution to converge for decreasing values of  $\Delta r$  as it does for decreasing  $\Delta t$ .

**Modeling spines** Calcium transients in spines have been modeled extensively to study the role of the  $Ca^{2+}$  influx through NMDA receptor channels (Mayer and Westbrook, 1987) in the induction of synaptic plasticity (Artola and Singer, 1993). Usually only one or a few spines are modeled in detail and coupled to a compartmental model of the dendritic tree.

Both the head and neck of the spine can be represented as a set of short cylinders stacked on top of each other (fig. 6.4), with the diffusion along the axis of the cylinders. Eq. 6.14 or 6.16 can again be applied, with:

$$C_{i,i+1} = \frac{1}{x^2} \quad \text{if } r_{i+1} \geq r_i \text{ and } \Delta x_i = \Delta x_{i+1} \quad (6.20)$$

between cylinders in the spine head or neck, and at the transition from head cylinder  $i$  to neck cylinder  $j$  the more general form:

$$C_{i,j} = \frac{2r_j^2}{r_i^2 \Delta x_i (\Delta x_i + \Delta x_j)} \quad (6.21)$$

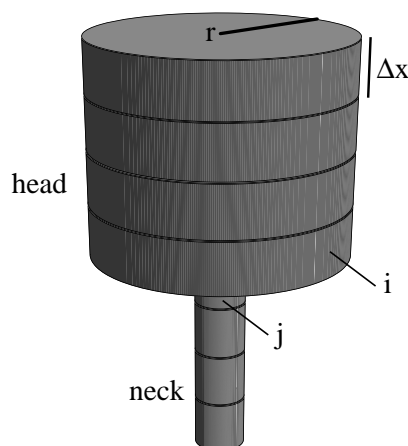


Figure 6.4: Diffusion is modeled in a spine by stacking short cylinders on top of each other. In this example the spine head is represented by 4 cylinders with  $\Delta x = 0.10 \mu m$  and  $r = 0.25 \mu m$  and the neck by 4 cylinders with  $\Delta x = 0.10 \mu m$  and  $r = 0.05 \mu m$ . One-dimensional diffusion is modeled along the  $X$  axis.

Eq. 6.21 assumes a sharp transition between the spine head and the neck. In practice eq. 6.21 works fine, though in several models the transition between head and neck has been modeled either as a large number of thin segments (Zador, Koch and Brown, 1990) or as a smooth function (Holmes and Levy, 1990).

**Examples of spine models** Koch and co-workers have implemented detailed models of  $Ca^{2+}$  transients in a spine coupled to simplified models of a hippocampal pyramidal neuron (Gamble and Koch, 1987; Zador, Koch and Brown, 1990). They showed that the voltage-dependent  $Ca^{2+}$  entry through the NMDA receptor channel can be the factor that couples pre- and postsynaptic activity during Hebbian learning at synapses (Hebb, 1949). Recently a phenomenological model of  $Ca^{2+}$  stores was added to this model by Schieg et al. (1995). Holmes and Levy (1990) studied induction of long term potentiation by simulating 100 spines on a detailed model of a dendate granule cell. GENESIS scripts for this model (De Schutter and Bower, 1993) can be downloaded from <http://bbf-www.uia.ac.be/CHAPTER/spine.html>.

### 6.4.2 Multi-dimensional diffusion

Calcium influx into presynaptic terminals causes localized increases in  $[Ca^{2+}]$  to hundreds of  $\mu M$  in regions just below the channel pores, called ‘microdomains’ (Llinás, Sugimori and Silver, 1992). Many models have simulated the  $[Ca^{2+}]$  in these domains to better understand the relation between  $Ca^{2+}$  entry and transmitter release (Parnas, Hovav and Parnas, 1989; Yamada and Zucker, 1992; Winslow, Duffy and Charlton, 1994). Such models require the simulation of

three-dimensional diffusion of  $Ca^{2+}$ . The terminal is discretized into many cubic boxes and diffusion is modeled as the summation of fluxes along each axis. For example, the diffusion along the  $X$  axis can be approximated as:

$$\frac{\partial^2 [Ca^{2+}]_{x,y,z,t}}{\partial x^2} \approx \frac{1}{\Delta x^2} ([Ca^{2+}]_{x-\Delta x,y,z,t} - 2[Ca^{2+}]_{x,y,z,t} + [Ca^{2+}]_{x+\Delta x,y,z,t}) \quad (6.22)$$

Applying similar equations along the  $Y$  and  $Z$  axes, one arrives at:

$$[Ca^{2+}]_{x,y,z,t+\Delta t} - [Ca^{2+}]_{x,y,z,t} = \Delta t D_{Ca} \left( \frac{\partial^2 [Ca^{2+}]_{x,y,z,t}}{\partial x^2} + \frac{\partial^2 [Ca^{2+}]_{x,y,z,t}}{\partial y^2} + \frac{\partial^2 [Ca^{2+}]_{x,y,z,t}}{\partial z^2} \right) \quad (6.23)$$

Eq. 6.23 is solved explicitly or using standard PDE solvers (Chapter 14). Boundary conditions are an important problem in multi-dimensional diffusion, because the simulated volume is often assumed to be part of a much larger volume without diffusional constraints. The standard solution is to model the complete volume where  $[Ca^{2+}]$  will be perturbed in detail and to add at the periphery (progressively) larger boxes until one reaches zones where  $[Ca^{2+}]$  remains at rest. Small time-steps are necessary (about 0.1  $\mu sec$ ) and even with adaptive box sizes, one easily ends up with millions of boxes (Yamada and Zucker, 1992). Such models obviously require very long computation times.

**Alternating Direction Implicit method** An elegant method to solve this problem is the ADI method (Press et al., 1992; Fletcher, 1991), which we will describe for the Crank-Nicholson formulation of two-dimensional diffusion in a cylinder. The cylinder is discretized into many annuli, which are shells divided into short segments along the  $X$  axis. Diffusion is described in a cylindrical coordinate system ( $r, \theta, x$ ; fig. 6.3) and the concentration function is considered cylindrically symmetric (i.e. independent of  $\theta$ ). Each time-step is divided into two steps of size  $\Delta t/2$  and in each sub-step a different independent variable is treated implicitly:

$$[Ca^{2+}]_{i,j,t+\Delta t/2} - [Ca^{2+}]_{i,j,t} = \frac{\Delta t}{4} D_{Ca} \left( C_{i,i+1} ([Ca^{2+}]_{i+1,j,t+\Delta t/2} - [Ca^{2+}]_{i,j,t+\Delta t/2}) + C_{j,j+1} ([Ca^{2+}]_{i,j+1,t} - [Ca^{2+}]_{i,j,t}) \right) \quad (6.24)$$

$$[Ca^{2+}]_{i,j,t+\Delta t} - [Ca^{2+}]_{i,j,t+\Delta t/2} = \frac{\Delta t}{4} D_{Ca} \left( C_{i,i+1} ([Ca^{2+}]_{i+1,j,t+\Delta t/2} - [Ca^{2+}]_{i,j,t+\Delta t/2}) + C_{j,j+1} ([Ca^{2+}]_{i,j+1,t+\Delta t} - [Ca^{2+}]_{i,j,t+\Delta t}) \right) \quad (6.25)$$

where first diffusion along the  $r$ -coordinate is solved implicitly ( $i$  variable in eq. 6.24) and then over the  $x$ -coordinate ( $j$  variable in eq. 6.25). Eqs. 6.24

and 6.25 are written like eq. 6.16, i.e. for diffusion to one side from  $i$  to  $i + 1$  and from  $j$  to  $j + 1$  only, but it should be obvious how to convert them to the form of eq. 6.17 which includes diffusion to both sides. Again, the two matrices corresponding to the systems of coupled equations of 6.24–6.25 are tridiagonal with diagonal dominance and can be solved very efficiently. In two dimensions, the ADI scheme for diffusion is unconditionally stable for the full time-step and second order accurate in both space and time, provided the appropriate boundary conditions are used (Fletcher, 1991). An example of the use of the two-dimensional ADI method with cylindrical coordinates can be found in a model of glutamate diffusion by Holmes (1995). The ADI scheme can also be used to model three-dimensional diffusion with sub-steps of  $\Delta t/3$ , but it is only conditionally stable (Fletcher, 1991).

The use of cylindrical coordinates allows a faithful representation of the geometry of the submembrane region, which is usually the most important one in neuronal models of diffusion. Unfortunately, modeling three-dimensional diffusion in cylindrical coordinates is awkward because the volume elements become extremely small close to the center. To simulate three-dimensional diffusion in a complex geometry like a spine, a finite element method might be indicated. These can be implemented using standard mathematical packages (e.g. Aharon, Parnas and Parnas 1994), but are again very computation intensive.

**Domain model** Finally, we repeat the message from section 6.2. It may not be necessary to model  $Ca^{2+}$  diffusion in three dimensions if the high concentrations inside the  $Ca^{2+}$  microdomains (Chad and Eckert, 1984; Llinás, Sugimori and Silver, 1992) are needed only to inactivate  $Ca^{2+}$  channels or to activate  $K^+$  channels or transmitter release. A highly simplified model sets the domain  $Ca^{2+}$  concentration directly proportional to the current through the  $Ca^{2+}$  channel (Sherman, Keizer and Rinzel, 1990):

$$[Ca^{2+}]_{d,i} = -\frac{\gamma}{a_i} I_{Ca,i} \quad (6.26)$$

where  $a_i$  normalizes the current for membrane surface and  $\gamma$  converts from units of current to concentration and incorporates any additional effects of diffusion and buffering. This model has obvious limitations and becomes inaccurate when the membrane potential approaches the reversal potential, but it is very fast.

## 6.5 Electro-diffusion models

In section 6.4.1 simple models of  $[Ca^{2+}]$  in a dendritic spine (Zador, Koch and Brown, 1990) were described. It was implicitly assumed that the voltage transients and the ionic concentrations in these models can be computed separately and interact only through the transmitter-gated ionic influx. But even relatively small ionic fluxes cause large changes in ionic concentration in the limited volume of a spine head (Koch and Zador, 1993) and change the ionic equilibrium potential. A first improvement is to use the Nernst equation (eq. 4.16), or even

better the constant field equation (eq. 6.6; Holmes and Levy 1990) to compute the synaptic current.

Qian and Sejnowski (1989) have argued, however, that this is not sufficient. Instead they proposed that concentrations in spines should be described by an electro-diffusion model based on the Nernst-Planck equation (Hille, 1991). If one again assumes only diffusion along the axis of the compartment cylinder, the Nernst-Planck equation for  $Ca^{2+}$  can be reduced to:

$$\frac{\partial[Ca^{2+}]}{\partial t} = D_{Ca} \frac{\partial^2[Ca^{2+}]}{\partial x^2} + D_{Ca} \frac{z_{Ca}F}{RT} \frac{\partial}{\partial x} \left( [Ca^{2+}] \frac{\partial V}{\partial x} \right) - \frac{1}{v} J_{Ca} \quad (6.27)$$

Eq. 6.27 states that  $[Ca^{2+}]$  can change due to pure diffusion (first term), the potential gradient (second term) and the transmembrane flux  $J_{Ca}$  (computed with the GHK equation, i.e. eq. 6.6). An additional equation is needed to compute the effect of changes in ionic concentration on the membrane potential and Qian and Sejnowski (1989) suggest using the total charge taken over the concentration of every ion inside a cylindrical compartment:

$$V(x, t) = V_{rest} + \frac{r}{2 C_m} F \sum_{ions} z_{ion} \left( [ion](x, t) - [ion]_{rest} \right) \quad (6.28)$$

where  $r$  is the radius and  $C_m$  the capacitance. Eq. 6.27 can be converted to a finite difference equation and solved together with eq. 6.28 using the forward Euler method, but the electro-diffusion system is quite computation intensive.

To circumvent this problem, the same authors have suggested a simple modification of the standard compartmental model (Chapter 3) that approximates the electro-diffusion model. Besides computing changes in concentration caused by transmembrane fluxes and using the GHK eq. (6.6) to compute ionic currents, the axial current is replaced by several axial fluxes caused by the electro-chemical gradients. Effectively, the axial current (compare to eq. 14.25) is decomposed into a series of parallel currents, one for each ionic species that is modeled:

$$C_m \frac{V_{i,t+\Delta t} - V_{i,t}}{\Delta t} = \sum_j \left( \frac{a_{i,j}}{2(\Delta x)^2} \sum_{ions} \frac{E_{i,j,ion} + V_{i,t} - V_{j,t}}{R_{i,ion}} \right) - \bar{g} V_{i,t} - \sum_{ions} I_{ion} \quad (6.29)$$

where  $a_{i,j}$  is the cross-sectional area coupling compartments  $i$  and  $j$ ,  $E_{i,j,ion}$  is the electrochemical driving force for each ion (computed as the Nernst potential between adjoining compartments) and  $R_{i,ion}$  is the coupling resistance for each ionic species, which needs to be computed at every time-step. For example for  $Ca^{2+}$ :

$$R_{i, Ca} = \frac{RT}{D_{Ca} z_{Ca} F} \frac{1}{z_{Ca} F [Ca^{2+}]_i} \quad (6.30)$$

Finally, the changes in concentration due to the ion specific axial currents need to be added to those caused by the membrane currents  $I_{ion}$ . Eqs. 6.29–6.30 give

a reasonable approximation of eq. 6.27, except during fast changes in transmembrane current (Qian and Sejnowski, 1989). The same reference also describes how to compute electro-diffusion at branches.

**Applicability and examples** Qian and Sejnowski (1989) suggest that the electro-diffusion equation (eq. 6.27), or its compartmental approximation (eq. 6.29), should be used whenever one wants to model electrical events in a structure with a diameter smaller than  $1 \mu m$ . They studied for example silent inhibition onto a spine. Cable modeling suggests that when a spine is contacted by both a  $Cl^-$  inhibitory synapse (reversal potential close to rest) and by an excitatory synapse, the inhibitory synapse can veto excitatory input by shunting the EPSP without producing a measurable IPSP (Koch, Poggio and Torre, 1982). This concept does not work in the electro-diffusion model because the inflow of  $Cl^-$  ions reduces the inhibitory reversal potential (Qian and Sejnowski, 1990). But as the different results in the electro-diffusion model can be explained by the use of the Nernst equation (eq. 4.16), it remains unclear if the computation of the axial electro-chemical flux (eq. 6.29) qualitatively changed the conclusion.

Moreover, the increased biophysical fidelity of the electro-diffusion model forces one to consider which charge carriers are responsible for the axial current. Qian and Sejnowski (1990) make the simple assumption that axial current is carried by the same ions as the transmembrane current, i.e.  $Na^+$ ,  $K^+$  and  $Cl^-$ . But is this correct? Many other ions and small molecules carry charge along the dendritic axis. Taking into account their mobility in water and their intraneuronal concentrations, the most important carriers are expected to be  $K^+$  ( $R_i$  of  $97 \Omega cm$  at  $20^\circ C$ ),  $Mg^{2+}$  ( $R_i$  of  $304 \Omega cm$ ) and phosphates ( $R_i$  of  $327 \Omega cm$ ) (Milazzo, 1963; Guyton, 1986; Hille, 1991). These  $R_i$  values assume that the ions are not buffered in the cytoplasm, which is unlikely for  $Mg^{2+}$  (Zhou and Neher, 1993). All other ions have cytoplasmic resistivities of more than  $2000 \Omega cm$  at rest. In fact, because these resistivities operate in parallel, neglecting all ions except for  $K^+$ ,  $Mg^{2+}$  and phosphates changes the cytoplasmic resistivity at rest only from  $55 \Omega cm$  to  $60 \Omega cm$ ! Obviously these values vary as the ionic concentrations change due to transmembrane fluxes, but the  $[Na^+]$  has to rise more than fivefold or the  $[Cl^-]$  tenfold to reduce its  $R_i$  below  $300 \Omega cm$ .

These simple calculations suggest that electro-diffusion models are not necessary to model spines or small dendrites. It is more important to use the GHK equation and to consider that most ligand-gated channels are permeable to multiple ions, e.g.  $Na^+$ ,  $K^+$  and  $Ca^{2+}$  ions permeate through the NMDA receptor channel (Mayer and Westbrook, 1987) and  $Cl^-$  and  $HCO_3^-$  through the GABA<sub>A</sub> receptor channel (Staley, Soldo and Proctor, 1995). Electro-diffusion theory has been successfully applied, however, in axonal models to study the effects of injury (van Egeraat and Wikswo, 1993).

## 6.6 Buffer Capacity and Buffer Diffusion

Until now we have only considered free diffusion. Most ions, in particular divalent ones like  $Ca^{2+}$  and  $Mg^{2+}$ , bind to cytoplasmic buffers (Thayer and Miller,

1990; Neher and Augustine, 1992; Zhou and Neher, 1993). We will elaborate the second-order buffering scheme introduced in Chapter 4:



It should be noted that eq. 6.31 is only an approximation as most  $Ca^{2+}$ -binding proteins have multiple binding sites with different  $f$  and  $b$  rates (Linse, Helmerson and Forsen, 1991) and require more complex equations to be modeled accurately. In practice, however, experimental data for the binding rates are often not available.

### 6.6.1 Buffer capacity

An important parameter for models of  $Ca^{2+}$  buffering is the buffer capacity, the fractional amount of bound  $Ca^{2+}$  per free  $Ca^{2+}$ :

$$\kappa = \frac{d[CaB]_i}{d[Ca^{2+}]_i} \quad (6.32)$$

The buffer capacity can be estimated using specific  $Ca^{2+}$  sensitive dye imaging procedures (Neher and Augustine, 1992; Zhou and Neher, 1993) and ranges from about 45 (98% of  $Ca^{2+}$  entering the cell is bound to the buffer) in chromaffin cells (Zhou and Neher, 1993) to more than 4000 (99.97%) in Purkinje cells (Llano, DiPolo and Marty, 1994). If endogenous buffers have a low affinity (high dissociation constant  $K_d = b/f$ ), which seems to be the case (Neher and Augustine, 1992), the total buffer concentration  $[B]_T$  can be estimated from  $\kappa$ :

$$\kappa \approx \frac{[B]_T}{K_d} \quad \text{if } [Ca^{2+}]_i \ll K_d \quad (6.33)$$

### 6.6.2 Buffer diffusion

Eq. 6.33 raises the issue of what the intracellular buffers and their  $K_d$  are. A related question is whether buffers are mobile or not. Zhou and Neher (1993) have estimated that about 25% of the buffer capacity in adrenal chromaffin cells is represented by slowly mobile buffers ( $D_B$  about  $1 \cdot 10^{-7} \text{ cm}^2 \text{ sec}^{-1}$ ). Additionally, they postulate that anorganic anions and small metabolites should act as highly mobile buffers ( $D_B$  of  $2 \cdot 10^{-6} \text{ cm}^2 \text{ sec}^{-1}$ ). The highly mobile buffer capacity could not be measured, but was estimated to be less than 15%. More important, most indicator dyes used in  $Ca^{2+}$  imaging experiments also act as highly mobile buffers. The effects of the indicator fura-2 on  $Ca^{2+}$  diffusion have been modeled extensively using explicit forward Euler methods (Sala and Hernandez-Cruz, 1990; Blumenfeld, Zablou and Sabatini, 1992) and are also briefly described in section 6.6.5.

To study the effects of diffusible buffers, eq. 6.16 and eq. 6.31 need to be combined. The implicit Crank-Nicholson equation for buffer diffusion is:

$$\begin{aligned}
& -\frac{\Delta t}{2} D_B C_{i-1,i} [B]_{i-1,t+\Delta t} \\
& + \left( 1 + \frac{\Delta t}{2} D_B (C_{i-1,i} + C_{i,i+1}) + \frac{\Delta t}{2} (b + f[Ca^{2+}]_{i,t}) \right) [B]_{i,t+\Delta t} \\
& + \frac{\Delta t}{2} f[B]_{i,t} [Ca^{2+}]_{i,t+\Delta t} - \frac{\Delta t}{2} D_B C_{i,i+1} [B]_{i+1,t+\Delta t} \\
& = \frac{\Delta t}{2} D_B C_{i-1,i} [B]_{i-1,t} \\
& + \left( 1 - \frac{\Delta t}{2} D_B (C_{i-1,i} + C_{i,i+1}) - \frac{\Delta t}{2} b \right) [B]_{i,t} \\
& + \frac{\Delta t}{2} D_B C_{i,i+1} [B]_{i+1,t} + \Delta t b [B]_{T,i}
\end{aligned} \tag{6.34}$$

where  $f$  and  $b$  are the forward and backward rates of the buffer binding reaction (eq. 6.31) and  $D_B$  is the diffusion constant of the buffer. Similarly for buffered  $Ca^{2+}$ -diffusion:

$$\begin{aligned}
& -\frac{\Delta t}{2} D_{Ca} C_{i-1,i} [Ca^{2+}]_{i-1,t+\Delta t} + \frac{\Delta t}{2} (b + f[Ca^{2+}]_{i,t}) [B]_{i,t+\Delta t} \\
& + \left( 1 + \frac{\Delta t}{2} D_{Ca} (C_{i-1,i} + C_{i,i+1}) + \frac{\Delta t}{2} f[B]_{i,t} \right) [Ca^{2+}]_{i,t+\Delta t} \\
& - \frac{\Delta t}{2} D_{Ca} C_{i,i+1} [Ca^{2+}]_{i+1,t+\Delta t} \\
& = \frac{\Delta t}{2} D_{Ca} C_{i-1,i} [Ca^{2+}]_{i-1,t} + \left( 1 - \frac{\Delta t}{2} D_{Ca} (C_{i-1,i} + C_{i,i+1}) \right) [Ca^{2+}]_{i,t} \\
& + \frac{\Delta t}{2} D_{Ca} C_{i,i+1} [Ca^{2+}]_{i+1,t} - \frac{\Delta t}{2} b [B]_{i,t} \\
& + \Delta t b [B]_{T,i} + \frac{\Delta t}{2} \frac{J_{i,t+\Delta t/2}}{v_i}
\end{aligned} \tag{6.35}$$

Eq. 6.34 assumes that  $[B]_{T,i}$  is constant, or in other words that  $D_B$  is identical for the free and bound forms of the buffer. This is a reasonable assumption taking into account the relative sizes of  $Ca^{2+}$  and most buffer molecules. Eqs. 6.34 and 6.35 should be solved together, resulting in a diagonally banded matrix with three bands for the  $Ca^{2+}$  diffusion and two bands extra for each buffer modeled. The most efficient ordering of the matrix is by shells, mixing  $[Ca^{2+}]$  and  $[B]$  so that the first row computes the buffer equations for the innermost shell. Because such a matrix is more complex to solve than the tridiagonal matrix of eq. 6.17, introducing buffers into a model will have an impact on computation speed.

### 6.6.3 Purkinje cell model

Radial diffusion of  $Ca^{2+}$  was modeled using concentric shells with a  $\Delta r$  of  $0.2 \mu m$ , resulting in a total of 7471 shells for the 1604 compartments in the

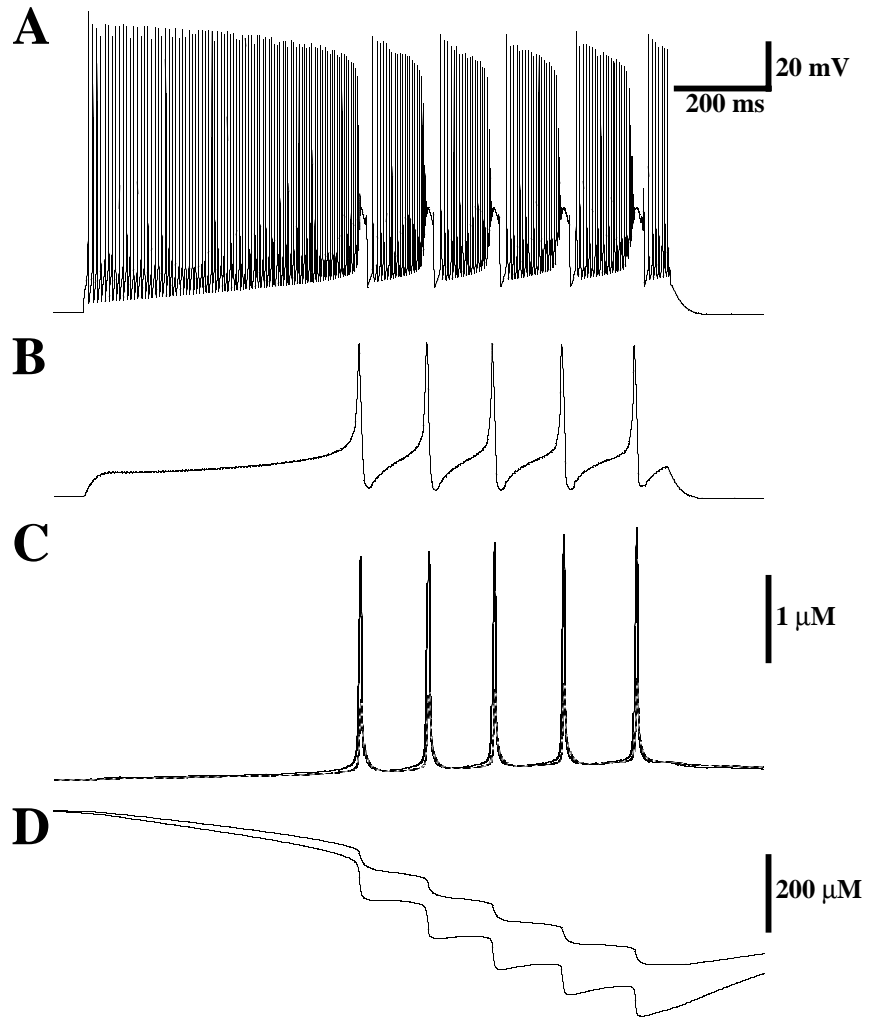


Figure 6.5: Response of the Purkinje cell model to a 1.2 sec long 1.5 nA current injection in the soma. **A.** Membrane potential in the soma shows that the model produces initially fast somatic  $Na^+$  spikes only. Later the dendrite starts spiking too. **B.** Membrane potential in a spiny dendrite demonstrates the initial plateau phase followed by dendritic  $Ca^{2+}$  spikes. **C.**  $[Ca^{2+}]$  in the submembrane (full line) and core shells (broken line) of the same spiny dendritic compartment, which has a diameter of 1.3  $\mu$ m. **D.** Free fixed buffer concentration in the same shells. During the current injection  $[B]$  decreased from 3.9 mM to 3.4 mM.

model. Usually simulations were run with a  $\Delta t$  of 10  $\mu\text{sec}$ , but to obtain an increased accuracy a  $\Delta t$  of 5  $\mu\text{sec}$  was used for the figures in this chapter.

We used a  $D_{Ca}$  of  $2 \cdot 10^{-6} \text{ cm}^2 \text{ sec}^{-1}$ . This value is 3 times slower than  $D_{Ca}$  in water (Chapter 4) and is based on measurements of  $Ca^{2+}$  diffusion rates in cytoplasm (Albritton, Meyer and Stryer, 1992). In general, diffusion constants listed in standard textbooks (e.g. Hille, 1991) apply to very dilute solutions, while cytoplasm is estimated to have twice the viscosity of water (Albritton, Meyer and Stryer, 1992).

A very high buffer capacity has been estimated for Purkinje cells (Llano, DiPolo and Marty, 1994). We have put the non-mobile buffer capacity at 2080 by including 4  $mM$  of a buffer with a  $K_d$  of 1.9  $\mu M$ . The relative slow binding rates ( $f = 1.3 \cdot 10^6 M^{-1} s^{-1}$ ) indicate that this buffer modeled  $Ca^{2+}$  uptake by both endogenous buffers and internal stores. Additionally we simulated fura-2, represented as 75  $\mu M$  of a mobile buffer ( $D_{fura} = 2 \cdot 10^{-6} \text{ cm}^2 s^{-1}$ ) with a  $K_d$  of 0.2  $\mu M$  ( $f = 4 \cdot 10^8 M^{-1} s^{-1}$ ). Buffer concentrations were identical in all shells. This is different from many other models where the submembrane shell had a higher buffer content (e.g. Chapter 4). While there is some evidence for higher submembrane buffer concentrations in cell bodies (Naraghi et al., 1995), this seems less likely to be the case for tiny dendritic branches.

**Results** Figure 6.5 shows the  $Ca^{2+}$  dynamics of the Purkinje cell model during a 1.5  $nA$  somatic current injection. While the somatic firing pattern looks very similar to that of the earlier Purkinje cell model (De Schutter and Bower, 1994a), the dendritic spiking pattern has improved considerably. In particular, dendritic spikes were sharper and had a larger amplitude. The steady state  $[Ca^{2+}]$  in between spikes rose to 200  $nM$ , which was closer to reported changes in  $[Ca^{2+}]$  during current injection (Lev-Ram et al., 1992) and higher than in the earlier model that used eq. 6.1 ( $[Ca^{2+}]$  of 100  $nM$ ).

The  $[Ca^{2+}]$  profiles showed a significant radial gradient in all compartments, which can be explained by the effect of the buffers on  $Ca^{2+}$  diffusion (see section 6.6.5). This was most obvious in the smooth dendrite (fig. 6.6A) where the submembrane shells sensed fast changes in  $Ca^{2+}$  inflow during somatic spikes, while the central core  $[Ca^{2+}]$  reflected highly attenuated dendritic spikes only. The gradient was less outspoken in the spiny dendrite shown in fig. 6.5C. The amount of free non-mobile buffer decreased progressively during long periods of bursting. This caused a slow rise of the steady state  $[Ca^{2+}]$ , leading by activation of  $K^+$  channels to a slower dendritic spiking.

#### 6.6.4 Modeling calcium indicator dyes

Whenever a biophysical model is built, it is important to constrain it with experimental data if available. In the case of  $Ca^{2+}$  dynamics, these are usually measurements using fluorescent indicator dyes. It is very important to realize that the use of such dyes distorts the  $Ca^{2+}$  signal in two ways. First, high affinity indicators like fura-2 have binding properties that affect the measured signal significantly. They are easy to saturate and their slow backward reaction

rate does not allow them to follow rapid  $[Ca^{2+}]$  changes. Regehr and Atluri (1995) compare the properties of high affinity dyes such as indo-1, fura-2, fluo-3 and calcium green-2 ( $K_d$  in the  $0.1 - 1 \mu M$  range) with those of low affinity dyes (furaptra and BTC). Second, these indicators act as mobile buffers, changing the  $Ca^{2+}$  dynamics themselves (Sala and Hernandez-Cruz 1990; Blumenfeld, Zablow and Sabatini 1992; Wagner and Keizer 1994).

Therefore it is impossible to directly compare the simulated  $[Ca^{2+}]$  transients with measured indicator signals. Instead, the indicator response itself should be modeled so that the experimentally estimated  $[Ca^{2+}]$  can be computed. We will describe the simulation of fura-2 indicators, which consists of three parts. It is trivial to apply similar methods to other indicators.

First, fura-2 must be included as a mobile buffer in the simulation of  $[Ca^{2+}]$  (section 6.6.2). This requires an estimate of  $[B]_T$  for fura-2, which is often impossible to measure experimentally, and of  $D_B$  and  $f$  and  $b$ . The last three factors depend on the ionic environment of the dye (Grynkiewicz, Poenie and Tsien, 1985) and values found in the literature vary a lot. For example,  $D_B$  values range from  $4 \cdot 10^{-7} cm^2 s^{-1}$  to  $2 \cdot 10^{-6} cm^2 s^{-1}$ ,  $f$  values from  $0.25 \cdot 10^8 M^{-1} s^{-1}$  to  $6.0 \cdot 10^8 M^{-1} s^{-1}$  and the, for distortions, more important values for the backward rate constant  $b$  from  $17 s^{-1}$  to  $380 s^{-1}$  (Timmermann and Ashley, 1986; Kao and Tsien, 1988; Blumenfeld, Zablow and Sabatini, 1992; Hollingworth et al., 1992; Zhou and Neher, 1993).

Next, the fluorescence emitted by bound and unbound fura-2 in response to excitation at  $340 nm$  ( $F_1$ ) or at  $380 nm$  ( $F_2$ ) (Grynkiewicz, Poenie and Tsien, 1985) must be computed in every shell  $i$ :

$$F_{j,i} = S_{b,j}[CaFura]_i + S_{f,j}[Fura]_i \quad j = 1, 2 \quad (6.36)$$

The  $S$  factors are measured experimentally using calibration solutions.  $S_{f,j}$  and  $S_{b,j}$  are the fluorescence measured as  $[Ca^{2+}]_i$  approaches zero ( $F_1$ ) or full saturation ( $F_2$ ) of fura-2 respectively. Typical values are:  $S_{b1} = 1.0 mM^{-1}$ ,  $S_{f1} = 0.455 mM^{-1}$ ,  $S_{b2} = 0.051 mM^{-1}$  and  $S_{f2} = 1.006 mM^{-1}$  (Blumenfeld, Zablow and Sabatini, 1992).

Finally, one needs to compensate for the limitations of the recording setup. Unless a confocal laser microscope was used, the measured excitation will be a spatial summation of different fluorescence levels throughout the radial axis of the cylinder (in the case of a dendrite). This means that the volume-weighted average should be computed over all shells  $i$  of the fluorescence levels  $F_{j,i}$ :

$$F_j = \frac{\sum_i v_i F_{j,i}}{\sum_i v_i} \quad j = 1, 2 \quad (6.37)$$

The total fluorescence levels  $F_1$  and  $F_2$  or their ratio can be compared directly to the measurements. Often the data are presented as an estimated  $[Ca^{2+}]$  (Grynkiewicz, Poenie and Tsien, 1985), which should then be computed also:

$$[Ca^{2+}]_{est} = K_{d,fura} \frac{S_{f2} F_1 / F_2 - S_{f1} / S_{f2}}{S_{b2} S_{b1} / S_{b2} - F_1 / F_2} \quad (6.38)$$

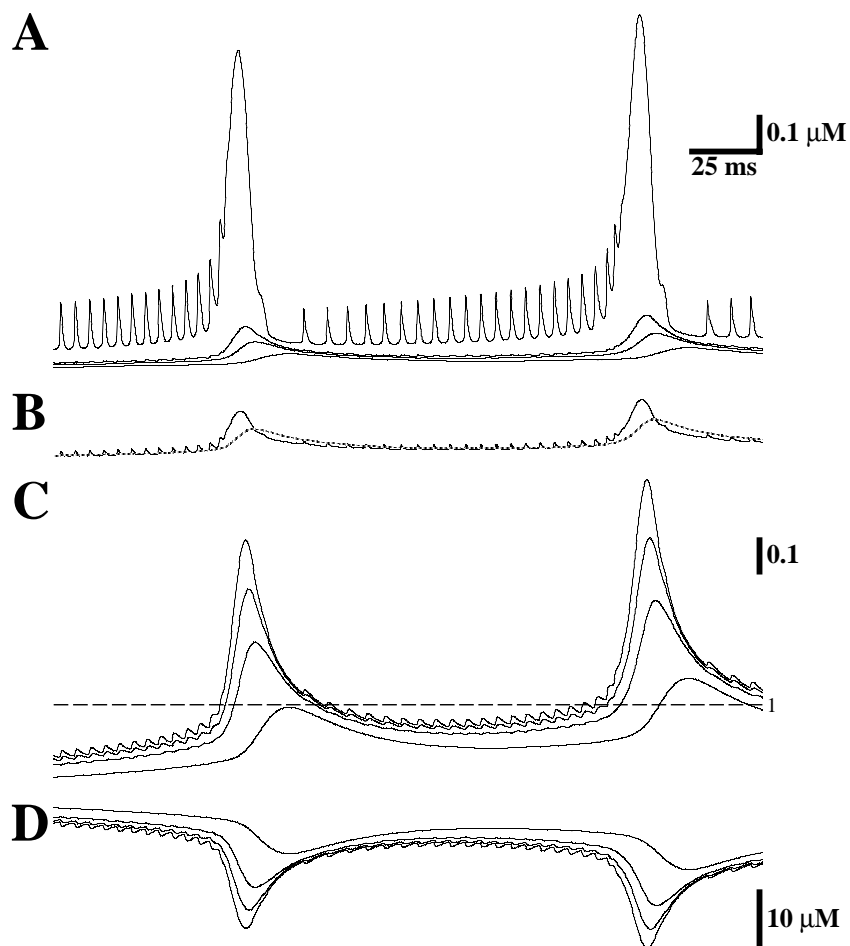


Figure 6.6: Simulation of fura-2 signals during the first two  $Ca^{2+}$  spikes of fig. 6.5. **A.** Calcium concentrations in a smooth dendritic compartment. The  $[Ca^{2+}]$  in the submembrane shell, in shells  $0.5 \mu m$  and  $1.0 \mu m$  below the membrane and in the core shell are shown. **B.** Spatial average of  $[Ca^{2+}]$  (full line) and the estimated  $[Ca^{2+}]$  (broken line) derived from the fura-2 signals (eq. 6.38) in the same compartment. **C.**  $F_1/F_2$  ratios in the same shells as shown in **A.** **D.** Free fura-2 concentrations in the same shells as in **A.** The free fura-2 decreased from about  $55 \mu M$  to about  $35 \mu M$  in the submembrane shell.

Many additional refinements to this fura-2 model are possible. For example, one can explicitly model the spatial blur and the temporal filtering of the recording system (Blumenfeld, Zablow and Sabatini, 1992) or the effect of background fluorescence and of  $Ca^{2+}$ -insensitive fura-2 (Zhou and Neher, 1993).

**Purkinje cell model** Fig. 6.6 shows a simulation of the fura-2 signal (using eqs. 6.36–6.38) in the smooth dendrite. As predicted, the fura-2 signal (fig. 6.6C) gave a filtered version of the  $[Ca^{2+}]$ . This is most obvious in the signal from the outer shell, where the somatic spikes were damped and the rise and decay phase of the dendritic spikes were slowed down significantly. Note that fura-2 did not saturate during the simulation (fig. 6.6D). The spatially averaged fura-2 signal (fig. 6.6B) was only a poor measure of the rich  $[Ca^{2+}]$  dynamics in the smooth dendrite as it approximated most the  $[Ca^{2+}]$  1.0  $\mu m$  submembrane. The approximation was better for a spiny dendritic compartment because of the smaller  $[Ca^{2+}]$  gradients and the absence of fast  $[Ca^{2+}]$  changes caused by the passively propagated somatic spikes (fig. 6.5C).

### 6.6.5 Predictions from linearized calcium theory

Several groups have developed simplified equations for buffered diffusion (Wagner and Keizer, 1994; Zador and Koch, 1994). We will briefly discuss the properties of the linearized  $Ca^{2+}$  theory (Zador and Koch, 1994), but its derivation is beyond the scope of this chapter.

If the  $[Ca^{2+}]$  is sufficiently small to neglect any buffer saturation ( $[Ca^{2+}] \ll K_d$ ) and if the buffering reaction can be considered to be at equilibrium with respect to the diffusional processes, one can describe buffered diffusion as:

$$\frac{r}{2}(1 + \kappa) \frac{\partial [Ca^{2+}](x, t)}{\partial t} = \frac{r}{2} (D_{Ca} + \kappa D_B) \frac{\partial^2 [Ca^{2+}](x, t)}{\partial x^2} - P_m [Ca^{2+}](x, t) + K_\infty P_m I_{Ca}(x, t) \quad (6.39)$$

where  $r$  is the radius of the cylinder,  $\kappa$  is defined in eq. 6.33 and  $P_m$  is the pump rate (units of  $m/sec$ ). The last term converts the  $Ca^{2+}$  current into concentration with  $K_\infty$  as a proportionality constant. The usefulness of eq. 6.39 for the solution of  $[Ca^{2+}]$  transients is limited (Zador and Koch, 1994), but it allows one to gain an intuitive feeling for axial diffusion in a cylinder. In fact, eq. 6.39 is identical in form to the equation for propagation of voltage along a one-dimensional fiber (Chapter 2):

$$C_m \frac{\partial V(x, t)}{\partial t} = \frac{r}{2R_i} \frac{\partial^2 V(x, t)}{\partial x^2} - \frac{1}{R_m} V(x, t) + \frac{R_\infty}{R_m} I_{Ca}(x, t) \quad (6.40)$$

By substituting the proper parameters, one can therefore define space and time constants for the  $Ca^{2+}$  reaction-diffusion system:

$$\lambda_{Ca} = \sqrt{\frac{r(D_{Ca} + \kappa D_B)}{2P_m}} \quad (6.41)$$

$$\tau_{Ca} = \frac{r(1 + \kappa)}{2P_m} \quad (6.42)$$

Comparison of eqs. 6.41 and 6.42 with the corresponding electrical  $\lambda$  and  $\tau$  (Chapter 2) produces useful insights into the properties of buffered diffusion. First, both the space and time constant depend on  $r$ , while the electrical time constant is independent of  $r$ . The effect of  $r$  on the dynamics of diffusion (eq. 6.42) is often described by experimentalists as the surface-to-volume ratio effect, which in effect states that the equilibration speed scales with  $2/r$  for a cylinder and with  $3/r$  for a sphere. Second, the space constant for  $Ca^{2+}$  and other second messengers is in general 1000 times smaller than the electrical space constant (Kasai and Petersen, 1994). Changes in  $[Ca^{2+}]$  tend therefore to stay much more localized within the dendritic tree than electrical transients, which has important consequences for  $Ca^{2+}$  signaling. The difference in  $\lambda$  also explains why diffusion shells should be much smaller than the spatial discretization needed for solving the non-linear cable equation. For example, in the Purkinje cell model the shells have a thickness of  $0.2 \mu m$  while the mean length for electrical compartments is  $7.5 \mu m$ . The space constant decreases with higher pump rates, as the pumps are equivalent to a membrane conductance in the voltage equation, but high diffusion constants have the opposite effect.

Finally, buffers can change both the capacity of the system and the effective diffusion rate. The capacity of the system is  $\frac{r}{2}(1 + [B]_T/K_d)$  (eq. 6.39). Without buffers the capacity is determined by the surface-to-volume ratio. Buffers increase the capacity of the system by an amount proportional to their total concentration (eq. 6.33) and to their affinity ( $1/K_d$ ). The effect of buffers on diffusion can be modeled as a change in the diffusion constant for  $Ca^{2+}$ . Neglecting the last two terms of eq. 6.39, and after dividing both sides by the capacity, an apparent diffusion coefficient (Wagner and Keizer, 1994; Zador and Koch, 1994) can be defined:

$$D_{app} \approx \frac{1}{1 + \kappa} D_{Ca} + D_B \quad \text{if } [Ca^{2+}]_i \ll K_d \text{ and } \kappa \gg 1 \quad (6.43)$$

The cytoplasmic  $D_{app}$  caused by the endogenous buffer capacity ( $\kappa$ ) of 45 or more (Neher and Augustine, 1992) is therefore expected to be more than an order of magnitude smaller than  $D_{Ca}$  in solution. For example, Albritton, Meyer and Stryer (1992) found that  $D_{app}$  was only  $1.3 \cdot 10^{-7} \text{ cm}^2 \text{ sec}^{-1}$  for buffered  $Ca^{2+}$  diffusion compared to  $2.2 \cdot 10^{-6} \text{ cm}^2 \text{ sec}^{-1}$  for free diffusion in cytoplasm. Diffusible buffers will increase  $D_{app}$  and  $\lambda_{Ca}$  because they transport  $Ca^{2+}$ . This is a consequence of the bound buffer generating a second concentration gradient besides the  $[Ca^{2+}]$  gradient (Sala and Hernandez-Cruz, 1990). The bound buffer will diffuse towards regions of low  $[CaB]$  which of course have also a low  $[Ca^{2+}]$  and this increases the apparent diffusion rate by  $D_B$  (eq. 6.43). Because  $D_B$  is not scaled by  $\frac{1}{1+\kappa}$  it will have a big effect on  $D_{app}$ , despite  $D_B$  being smaller than  $D_{Ca}$ .

Wagner and Keizer (1994) have shown that the effects on  $D_{app}$  are actually more complex, especially for high affinity buffers like fura-2. If enough mobile buffer is present to prevent immediate saturation, it will first bind  $Ca^{2+}$  without releasing it and it will have a capacitative effect only. Later, when enough  $Ca^{2+}$  is bound, the mobile buffer will start to release  $Ca^{2+}$  and the diffusive effect

becomes apparent. This means that  $D_{app}$  will increase over time.

This last point demonstrates the importance of buffer saturation, something linearized  $Ca^{2+}$  theory cannot predict. A systematic modeling study was done by Nowycky and Pinter (1993), who found that the submembrane transients during  $Ca^{2+}$  influx were shaped much more by the forward rate factor  $f$  than by  $K_d$ . Moreover, if fixed  $[CaB]$  could be measured, this would give a much better representation of the spatial  $[Ca^{2+}]$  gradient than diffusible  $[CaB]$  (e.g. fura-2). Finally, during fast changes in  $[Ca^{2+}]$  other  $Ca^{2+}$ -binding proteins that have fast binding rates, e.g. calmodulin (Linse, Helmerson and Forse, 1991), will compete with the indicator dye and cause it to bind less  $Ca^{2+}$ . This may lead to an underestimate of the  $Ca^{2+}$  influx in experiments where this influx is measured by the use of very high concentrations of fura-2 (Tempia et al., 1995).

## 6.7 Uptake and release from calcium stores

Calcium release from intracellular stores plays a central role in the generation of  $Ca^{2+}$  oscillations and  $Ca^{2+}$  waves (Berridge, 1993).  $Ca^{2+}$  oscillations are cyclic changes in the cytoplasmic  $[Ca^{2+}]$  caused by repetitive periods of release of  $Ca^{2+}$  from stores, followed each time by re-uptake. Cytoplasmic  $Ca^{2+}$  waves are the spatial transmission of similar processes. Because of their ubiquitous nature, these processes have generated tremendous interest from both experimentalists and modelers, but frequently outside the context of the nervous system. The models differ in the relative roles attributed to different release mechanisms in maintaining oscillations (Goldbeter, Dupont and Berridge, 1990; De Young and Keizer, 1992) and in  $Ca^{2+}$  versus  $IP_3$  diffusion in generating waves (Safri and Keizer, 1995; Sneyd et al., 1995); details which are beyond the scope of this chapter. It is important to realize, however, that these phenomena are much slower than most neuronal signals, with timescales of seconds and beyond.

Two separate mechanisms cause release from intracellular stores:  $Ca^{2+}$ -induced  $Ca^{2+}$  release (CICR) and  $IP_3$ -induced  $Ca^{2+}$  release (Berridge, 1993). CICR is mediated by a receptor which binds the muscle-paralyzing alkaloid ryanodine and which is activated by caffeine (Coronado et al., 1994).  $IP_3$  is a second messenger created by the hydrolysis of lipid precursors. This hydrolysis is stimulated by the activation of G protein-linked receptors like the metabotropic glutamate receptor (Schoepp and Conn, 1993). Calcium uptake into the stores is mostly by a  $Ca^{2+} - ATPase$  pump (Lytton et al., 1992). Recent measurements suggest that free  $[Ca^{2+}]$  in the stores is in the  $100 \mu M$  (Hofer and Machen, 1993) to  $5 mM$  range (Kendall, Dormer and Campbell, 1992). Stores contain large amounts of low affinity buffers like calsequestrin (Takei et al., 1992) and calretinin.

In Purkinje cells, the  $Ca^{2+}$  stores are part of the endoplasmic reticulum (ER). As the ryanodine and  $IP_3$  receptors have differential distributions, it has been suggested that the ER is subcompartmentalized into separate pools (Takei et al., 1992). Anatomical studies suggest, however, that the ER is one contiguous structure throughout the whole cell (Martone et al., 1993; Terasaki et al., 1994).

### 6.7.1 Calcium uptake and CICR

Goldbeter, Dupont and Berridge (1990) were first to describe a model of CICR-mediated  $[Ca^{2+}]$  oscillations which is still used extensively (Sneyd, Charles and Sanderson, 1994). These models give reasonable approximations of slow changes in  $[Ca^{2+}]$ , but they have several limitations in the context of simulating neuronal  $Ca^{2+}$  transients. First, both the  $Ca^{2+}$  uptake flux  $J_U$  and the release flux  $J_{CICR}$  are described phenomenologically by Hill functions (e.g. eq. 6.45), in other words the binding of  $Ca^{2+}$  to pumps and receptors is assumed fast enough to be at equilibrium. This assumption of steady-state kinetics is a sensible simplification at time scales of seconds, but experiments using caged release of  $Ca^{2+}$  have measured a time constant for activation of CICR of 1.1 msec (Györke and Fill, 1993). A second problem with the approach of Goldbeter and colleagues is that they assume that CICR ends because of depletion of the pool. Their model works only if the store concentration  $[Ca^{2+}]_s$  is in the low  $\mu M$  range, which is unlikely (Hofer and Machen, 1993; Kendall, Dormer and Campbell, 1992). We have assumed release to have a threshold and a lower affinity (Györke and Fill, 1993) than uptake, so that uptake will compensate release once the cytoplasmic  $[Ca^{2+}]_i$  increases sufficiently. Slow inactivation of release (Györke and Fill, 1993) was neglected. As a first step to more realistic kinetics for the  $Ca^{2+}$  uptake and CICR processes, we let the fluxes relax to the steady-state Hill function with a fixed time constant:

$$\frac{dJ_k([Ca^{2+}], t)}{dt} = \frac{J_{k,\infty}([Ca^{2+}]) - J_k([Ca^{2+}], t)}{\tau_k} \quad (6.44)$$

with  $k = U, CICR$

$$J_{U\infty} = V_U \frac{[Ca^{2+}]_i^2}{K_U^2 + [Ca^{2+}]_i^2} \quad (6.45)$$

$$J_{CICR\infty} = V_{CICR} \frac{[Ca^{2+}]_i}{K_{CICR} + [Ca^{2+}]_i} ([Ca^{2+}]_s - [Ca^{2+}]_i) \quad (6.46)$$

$$J_{CICR\infty} = 0.0 \text{ for } [Ca^{2+}]_i \leq K_T \quad (6.47)$$

where  $V_U$  and  $V_{CICR}$  are the maximum rates of uptake and release respectively. The parameters to eqs. 6.44–6.46 can be found in Appendix B. Eq. 6.45 describes the steady-state kinetics of many different types of  $Ca^{2+} - ATPase$  pumps, which are all activated cooperatively by  $Ca^{2+}$  with a Hill coefficient of 2 (Lytton et al., 1992). A limitation of eq. 6.45 is that it does not depend on  $[Ca^{2+}]_s$ , while empty stores have a higher rate of uptake (Missiaen et al., 1990).

### 6.7.2 $IP_3$ -induced calcium release

The  $IP_3$  receptor seems to have more complex dynamics than the ryanodine receptor. It has a bell-shaped steady-state curve for dependence on  $[Ca^{2+}]$  with a sharp peak around 0.2  $\mu M$  (Bezprozvanny, Watras and Ehrlich, 1991). De Young and Keizer (1992) have proposed a model for  $IP_3$  receptor gating which includes  $IP_3$ -binding steps and  $Ca^{2+}$ -activation and inactivation steps,

resulting in 8 possible states. This model was later reduced by Li and Rinzel (1994) to a Hodgkin-Huxley like formulation with an activation gate  $m$  and an inactivation gate  $h$ . Their set of equations can be incorporated easily into neuronal models. We have again adapted this formulation to include a time constant for the combined  $IP_3$  and  $Ca^{2+}$  activation.

$$J_{IP_3} = V_{IP_3} m^3 h^3 ([Ca^{2+}]_s - [Ca^{2+}]_i) \quad (6.48)$$

$$m_\infty = \frac{[IP_3]_i}{[IP_3]_i + d_{IP_3}} \frac{[Ca^{2+}]_i}{[Ca^{2+}]_i + d_{act}} \quad (6.49)$$

$$\tau_m = \frac{1}{b_{IP_3} + a_{IP_3} [Ca^{2+}]_i} \quad (6.50)$$

$$h_\infty = \frac{Q([IP_3])}{Q([IP_3]) + [Ca^{2+}]_i} \quad (6.51)$$

$$\tau_h = \frac{1}{a_{inh}(Q([IP_3]) + [Ca^{2+}]_i)} \quad (6.52)$$

$$Q = d_{inh} \frac{[IP_3]_i + d_{IP_3}}{[IP_3]_i + d_{dis}} \quad (6.53)$$

where  $V_{IP_3}$  is the maximum rate of  $IP_3$ -induced release. The parameters to eq. 6.48- 6.52 and a brief description of the different variables are summarized in Appendix B. A similar set of equations can be found in Sneyd et al. (1995).

**$IP_3$  concentration** Most models have assumed that  $[IP_3]$  increases are pulsatile and degradation follows linear (De Young and Keizer, 1992) or saturable kinetics (Sneyd et al., 1995). In neuronal models, where  $IP_3$  is generated by activation of the metabotropic glutamate receptor (Llano et al., 1991), it seems most appropriate to model the generation of  $IP_3$  with an alpha function:

$$\frac{d[IP_3]_i}{dt} = \gamma t e^{-t/t_{peak}} - \beta ([IP_3]_i - [IP_3]_{min}) \quad (6.54)$$

where  $t_{peak}$  is the time to peak,  $\gamma$  determines the maximum amount of  $IP_3$  production and  $\beta$  is the removal rate. More complex models have also included diffusion of  $IP_3$  and the positive feedback of  $[Ca^{2+}]$  onto  $IP_3$  production (De Young and Keizer, 1992).

### 6.7.3 The complete model of release from stores

Combining eqs. 6.44-6.54 gives a set of equations describing the change of  $[Ca^{2+}]$  in the cytoplasm:

$$\begin{aligned} \frac{\partial [Ca^{2+}]_i}{\partial t} = & D_{Ca} \frac{\partial^2 [Ca^{2+}]_i}{\partial x^2} + (b[CaB]_i - f[Ca^{2+}]_i[B]_i) \\ & + \frac{J_{CICR} + J_{IP_3} - J_U + V_{leak} ([Ca^{2+}]_s - [Ca^{2+}]_i)}{v_i} \end{aligned} \quad (6.55)$$

The first and second terms of eq. 6.55 represent the diffusive and buffering term from eq. 6.35. The last term describes all the store-related fluxes and a

leak flux with a constant rate  $V_{leak}$ . This leak flux is important to compensate the  $Ca^{2+}$  uptake by  $J_U$  at rest. An equation similar to eq. 6.55, but without the diffusive term and with the fluxes reversed, describes the change of  $[Ca^{2+}]_s$ . During the implicit solution of the reaction-diffusion system the last term is evaluated at  $t + \Delta t/2$  (like the Hodgkin-Huxley equations, see Section 14.3.6).

Eq. 6.55 implicitly assumes that the  $Ca^{2+}$  fluxes do not change the electrical gradient across the ER membrane. The sarcoplasmic reticulum, which is a specialized ER found in muscle, has a membrane potential of about  $+20$  mV compared to the cytoplasm (Stephenson, Wendt and Forrest, 1981). Jafri and Gillo (1994) have made a model where eq. 6.44–6.46 are used to compute a  $\bar{v}$  which combined with the Nernst potential (eq. 4.16) across the ER membrane gives a  $Ca^{2+}$  current. This model produced correct ER membrane potentials only if the movement of counterions like  $K^+$  into the ER was included also.

**Purkinje cell model** The Purkinje cell model presented so far did not contain  $Ca^{2+}$  stores. Fig. 6.7 presents some preliminary results of a model where a  $Ca^{2+}$  store was included in every shell. Based on an electronmicroscopic reconstruction of the ER in Purkinje cells (Martone et al., 1993), the stores were assumed to occupy 20% of the volume of each shell. This store volume was converted into store surface using the assumption that the ER could be represented as a long tube with a diameter of  $0.050$   $\mu m$  (Palay and Chan-Palay, 1974).

In practice we found that beyond the limitations imposed by the use of Hill functions in eqs. 6.44–6.46, the CICR model was also very sensitive to the values of its parameters, most of which are not better than educated guesses (Appendix B). In particular, CICR produced reasonable results only if calsequestrin was assumed to have extremely slow backward binding rates ( $b$  of 1 to 10  $sec^{-1}$ ). With faster rates CICR dumped the complete contents of the stores fast enough to raise the cytoplasmic  $[Ca^{2+}]$  beyond  $20$   $\mu M$ . We used also higher threshold values ( $K_T = 200$  nM) than reported for Purkinje cells (Kano et al., 1995), because the experimental values are distorted by the spatial averaging of the fura-2 signal (fig. 6.6B). In fact, the apparent  $[Ca^{2+}]$  threshold for CICR that can be estimated from the computed fura-2 signal in a spiny dendrite of the model ( $80$  nM) is very close to the experimental values (Kano et al., 1995).

We have tuned the parameters of the CICR model so that CICR is activated during somatic current injection without causing noticeable changes to the Purkinje cell firing pattern (fig. 6.7A). In comparison with the Purkinje cell model without  $Ca^{2+}$  stores (fig. 6.5A) the firing pattern looks similar and the subtle differences are within the normal range. This corresponds to the experimental observation that firing patterns look normal in cells where subsequent addition of low concentrations of caffeine evokes large  $Ca^{2+}$  signals due to CICR. Nevertheless, CICR caused complex changes to the cytoplasmic  $Ca^{2+}$  levels during the dendritic spikes (fig. 6.7B). Each dendritic spike evoked CICR, causing prolonged increases of the submembrane  $[Ca^{2+}]$ . Note that the first dendritic spike was initiated sooner due to the CICR itself. The CICR remained localized to the submembrane region, it did not cause a  $Ca^{2+}$  wave traveling towards the center of the compartment. This can be explained by the

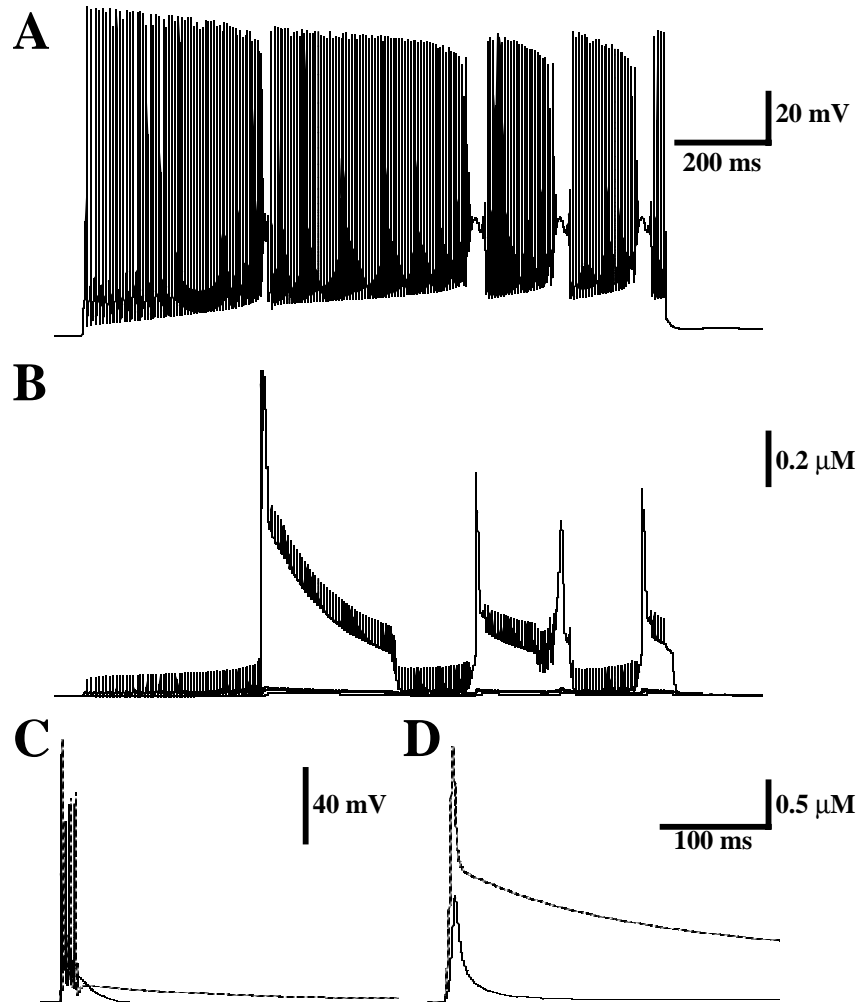


Figure 6.7:  $Ca^{2+}$ -induced  $Ca^{2+}$  release in the Purkinje cell model. **A.** Membrane potential in the soma during a 1.5 nA somatic current injection. **B.**  $Ca^{2+}$  concentrations in the same shells of a smooth dendritic compartment as in fig. 6.6A. **C.** Comparison of somatic membrane potentials during a complex spike in model without (full line) and with  $Ca^{2+}$  stores (broken line). The subtle differences in spiking during the initial burst are functionally not significant, but the subsequent plateau depolarization in the  $Ca^{2+}$  store model is. **D.** Fura-2 estimated  $[Ca^{2+}]$  in a spiny dendrite during the same complex spikes.

relative high threshold for CICR initiation ( $K_T$ ).

Using the same parameters, CICR had a profound effect on the shape of the complex spike (fig. 6.7C). The complex spike is a distributed synaptic response evoked by climbing fiber stimulation that activates  $Ca^{2+}$  channels everywhere in the dendritic tree (Miyakawa et al., 1992). In the presence of  $Ca^{2+}$  stores the increase in  $[Ca^{2+}]$  due to  $Ca^{2+}$  infow was markedly enhanced by CICR (fig. 6.7D). This activated the  $Na^+-Ca^{2+}$  exchanger, causing the prolonged depolarization in the model with CICR. Depolarizing plateaus evoked by complex spikes have been reported in the literature (Ekerot and Oscarsson, 1981).

## 6.8 Conclusions

This chapter has given an overview of up-to-date techniques to model biophysically realistic  $Ca^{2+}$  dynamics in a compartmental model of a dendritic tree. Many of these techniques can easily be applied to the simulation of other ionic species or of second messengers.

The model we have presented is a first step towards understanding the role of  $Ca^{2+}$  release in Purkinje cell physiology. Over the coming years we expect the model to become more complex. We have neglected, for example, diffusion of  $IP_3$  and we have modeled radial diffusion of  $Ca^{2+}$  only. Because of buffering,  $Ca^{2+}$  has a very low  $D_{app}$ , so that one can assume that it has little longitudinal effects. This may not be true for  $Ca^{2+}$  release mechanisms, however. Because  $IP_3$  is not buffered, it is expected to diffuse much further than  $Ca^{2+}$  (Kasai and Petersen, 1994; but see Wang and Augustine, 1995) and it has been hypothesized that CICR could transmit  $Ca^{2+}$  gradients down a dendrite (Sah, 1996). We have also neglected the morphology of the ER and other organelles in the cytoplasm, which can obstruct diffusion (Kargacin, 1994). Nor are release mechanism expected to be uniformly distributed (Martone et al., 1993).

Finally, how can  $[Ca^{2+}]$  in spines be modeled correctly? A quick calculation shows that a 25 nM concentration corresponds to exactly one ion in the volume of a 0.5  $\mu m$  diameter sphere, which is about the size of a spine head! This raises doubt about the use of differential equations to describe  $[Ca^{2+}]$  in spines. A Monte Carlo method might be more appropriate in this context. An example is the study of transmitter diffusion by Bartol et al. (1991). We believe that Monte Carlo methods might be the best technique to study  $[Ca^{2+}]$  diffusion in 3 dimensions (Bormann and De Schutter, 1996).

The authors' address is Theoretical Neurobiology, Born-Bunge Foundation, University of Antwerp, B2610 Antwerp, Belgium. Erik De Schutter can be e-mailed at erik@bbf.uia.ac.be. This research is supported by NIMH grant 1-R01-MH52903 and by ESF grant 156. E. De Schutter is a research fellow of the Belgian National Fund for Scientific Research. The authors thank Guy Bormann for his help in the conversion to LATEX and Christof Koch, Reinoud Maex and Alex Protopapas for comments on earlier versions of this chapter.

## Appendix 6.A: Purkinje cell model description

The equations and parameters specific to the simulation of  $[Ca^{2+}]$  dynamics are presented in this chapter and in Appendix B. For the sake of brevity we will not list all the parameters for the passive properties of the model and for the voltage-gated channels. The complete Purkinje cell model can be obtained at <http://bbf-www.uia.ac.be/CHAPTER/Purkinje.html>.

The model simulates the same morphology as the earlier one (De Schutter and Bower, 1994a) except for the addition of an axon hillock 4 compartments long. This makes 1604 the total number of compartments. The membrane capacitance was changed to  $1 \mu F cm^{-2}$ , which is the standard value used in most models (Jack, Noble and Tsien, 1975).

All the compartments in the model are active. Channel kinetics are simulated using Hodgkin-Huxley-like equations and a similar set of 9 channel types as before was used. The soma has fast and persistent  $Na^+$  channels (NaF and NaP), T-type and P-type  $Ca^{2+}$  channels (CaT and CaP), a delayed rectifier (Kdr), an A-current (KA), non-inactivating  $K^+$  channels (KM) and an anomalous rectifier (Kh). The dendritic membrane includes CaT and CaP channels, a  $Ca^{2+}$ -activated  $K^+$  channel (KC) and a KM channel. Additionally, a transitional zone called the main dendrite also contains Kdr and KA channels. The axon hillock has NaF and Kdr channels in a slightly higher density than the soma. The total number of channels and pumps in the model without stores is 9842.

The Hodgkin-Huxley-like equations for the CaP and KA channel were updated, based on newer data from Purkinje cells. The conductance of the KC channel in the earlier model did not have a realistic dependence on  $[Ca^{2+}]$  (De Schutter and Bower, 1994a). Therefore the equation for KC was replaced by the kinetic description of a rat muscle BK channel (Moczydlowski and Latorre, 1983). These equations were based on measurements of channels incorporated in artificial lipid bilayers, a procedure which is known to affect the  $Ca^{2+}$  affinity of the channel (Kapicka et al., 1994). We therefore increased the affinity in the model by a factor 33 (e.g. Gabbiani et al., 1994), bringing it closer to the values for maximal KC activation measured in whole cells (Prakriya et al. 1996).

## Appendix 6.B: Parameters for calcium stores

$Ca^{2+}$ -uptake parameters (eq. 6.45):

$$V_U = 4 \cdot 10^{-9} \mu M cm^{-2} ms^{-1} \quad K_U = 1.0 \mu M \quad \tau_U = 1.0 ms$$

$Ca^{2+}$ -induced  $Ca^{2+}$  release parameters (eq. 6.46):

$$\begin{aligned} V_{CICR} &= 3 \cdot 10^{-8} cm^{-2} ms^{-1} & \tau_{CICR} &= 1.2 ms \\ K_{CICR} &= 0.3 \mu M & K_T &= 0.2 \mu M \end{aligned}$$

$IP_3$ -induced  $Ca^{2+}$  release parameters (eqs. 6.48–6.53):

$a$  are forward and  $b$  backward binding rate constants for  $IP_3$  receptor binding ( $a_{IP_3}$  and  $b_{IP_3}$ ) and inhibitive  $Ca^{2+}$  binding to the receptor ( $a_{inh}$ ). Similarly, dissociation constants ( $b/a$ ) are defined for  $IP_3$  binding to the uninhibited ( $d_{IP_3}$ ) and  $Ca^{2+}$ -inhibited receptor ( $d_{dis}$ ), and for  $Ca^{2+}$ -activation ( $d_{act}$ ) and inhibition ( $d_{inh}$ ) of the receptor.

$$\begin{aligned} V_{IP_3} &= 1.0 \cdot 10^{-8} \text{ cm}^{-2} \text{ ms}^{-1} & b_{IP_3} &= 4.1 \cdot 10^{-3} \text{ ms}^{-1} \\ a_{inh} &= 2.0 \cdot 10^{-4} \text{ } \mu\text{M ms}^{-1} & a_{IP_3} &= 0.42 \text{ } \mu\text{M}^{-1} \text{ ms}^{-1} \\ d_{inh} &= 1.05 \text{ } \mu\text{M} & d_{IP_3} &= 0.13 \text{ } \mu\text{M} \\ d_{act} &= 8.2 \cdot 10^{-2} \text{ } \mu\text{M} & d_{dis} &= 0.94 \text{ } \mu\text{M} \end{aligned}$$

Initial  $Ca^{2+}$  concentrations:

$$[Ca^{2+}]_{i,rest} = 40 \text{ nM} \quad [Ca^{2+}]_{s,rest} = 200 \text{ } \mu\text{M}$$

Buffer in store (calsequestrin) parameters:

$$K_d = 1 \text{ } \mu\text{M} \quad f_s = 10 \text{ M}^{-1} \text{ ms}^{-1} \quad b_s = 0.01 \text{ ms}^{-1} \quad [B]_{T,s} = 100 \text{ } \mu\text{M}$$

## References

- Aharon, S., Parnas, H., and Parnas, I. (1994) The magnitude and significance of  $Ca^{2+}$  domains for release of neurotransmitter. *Bull. Math. Biol.* **56**: 1095-1119.
- Aidley, D.J. (1991) *The Physiology of Excitable Cells*. Cambridge University Press, Cambridge.
- Albritton, M.L., Meyer, T., and Stryer, L. (1992) Range of messenger action of calcium ion and inositol 1,4,5-triphosphate. *Science* **258**: 1812-1815.
- Angstadt, J.D., and Calabrese, R.L. (1991) Calcium currents and graded synaptic transmission between heart interneurons of the leech. *J. Neurosci.* **11**: 746-759.
- Artola, A., and Singer, W. (1993) Long-term depression of excitatory synaptic transmission and its relationship to long-term potentiation. *Trends Neurosci.* **16**: 480-487.
- Augustine, G.J., Charlton, M.P., and Smith, S.J. (1985) Calcium entry and transmitter release at voltage-clamped nerve terminals of squid. *J. Physiol. (London)* **367**: 163-181.
- Bartol, T.M., Land, B.R., Salpeter, E.E., and Salpeter, M.M. (1991) Monte Carlo simulation of miniature end-plate current generation in the vertebrate neuromuscular junction. *Biophys. J.* **59**: 1290-1307.
- Bernander, Ö., Douglas, R.J., Martin, K.A.C., and Koch, C. (1991) Synaptic background activity influences spatiotemporal integration in single pyramidal cells. *Proc. Natl. Acad. Sci. USA* **88**: 11569-11573.
- Berridge, M.J. (1993) Inositol triphosphate and calcium signalling. *Nature* **361**: 315-325.
- Bezprozvanny, I., Watras, J., and Ehrlich, B.E. (1991) Bell-shaped calcium-dependent curves of ins(1,4,5)P<sub>3</sub>-gated and calcium-gated channels from endoplasmic reticulum of cerebellum. *Nature* **351**: 751-754.
- Blumenfeld, H., Zablow, L., and Sabatini, B. (1992) Evaluation of cellular mechanisms for modulation of calcium transients using a mathematical model of fura-2  $Ca^{2+}$  imaging in Aplysia sensory neurons. *Biophys. J.* **63**: 1146-1164.
- Bormann, G., and De Schutter, E. (1996) Monte Carlo simulation of 3D calcium diffusion in detailed neuronal models. *2nd Meeting Europ. Neurosci.* 13.
- Bower, J.M., and Beeman, D. (1995) *The Book of GENESIS: Exploring Realistic Neural Models with the GENeral NEural SIMulation System*. TELOS, New York, NY.
- Buchholtz, F., Golowasch, J., Epstein, I.R., and Marder, E. (1992) Mathematical model of an identified stomatogastric ganglion. *J. Neurophysiol.* **67**: 332-340.
- Calabrese, R.L., and De Schutter, E. (1992) Motor pattern generating networks in invertebrates: modeling our way toward understanding. *Trends Neurosci.* **15**: 439-445.
- Carnevale, N.T., and Rosenthal, S. (1992) Kinetics of diffusion in a spherical cell. I. No solute buffering. *J. Neurosci. Meth.* **41**: 205-216.

- Chad, J.E., and Eckert, R. (1984) Calcium domains associated with individual channels can account for anomalous voltage relations of Ca-dependent responses. *Biophys. J.* **45**: 993-999.
- Coronado, R., Morrissette, J., Sukhareva, M., and Vaughan, D.M. (1994) Structure and function of ryanodine receptors. *Amer. J. Physiol.* **266**: C1485-C1504.
- De Schutter, E. (1992) A consumer guide to neuronal modeling software. *Trends Neurosci.* **15**: 462-464.
- De Schutter, E. (1995) Dendritic calcium channels amplify the variability of postsynaptic responses. *Abstr. Soc. Neurosci.* **21**: 586.
- De Schutter, E., Angstadt, J.D., and Calabrese, R.L. (1993) A model of graded synaptic transmission for use in dynamic network simulations. *J. Neurophysiol.* **69**: 1225-1235.
- De Schutter, E., and Bower, J.M. (1993) Sensitivity of synaptic plasticity to the  $Ca^{2+}$  permeability of NMDA channels: a model of long-term potentiation in hippocampal neurons. *Neural Comput.* **5**: 681-694.
- De Schutter, E., and Bower, J.M. (1994a) An active membrane model of the cerebellar Purkinje cell. I. Simulation of current clamps in slice. *J. Neurophysiol.* **71**: 375-400.
- De Schutter, E., and Bower, J.M. (1994b) An active membrane model of the cerebellar Purkinje cell: II. Simulation of synaptic responses. *J. Neurophysiol.* **71**: 401-419.
- De Schutter, E., and Bower, J.M. (1994c) Simulated responses of cerebellar Purkinje cells are independent of the dendritic location of granule cell synaptic inputs. *Proc. Natl. Acad. Sci. USA* **91**: 4736-4740.
- De Young, G.W., and Keizer, J. (1992) A single-pool inositol-1,4,5-triphosphate-receptor-based model for agonist-stimulated oscillations in  $Ca^{2+}$  concentration. *Proc. Natl. Acad. Sci. USA* **89**: 9895-9899.
- Denk, W., Sugimori, M., and Llinás, R.R. (1995) 2 types of calcium response limited to single spines in cerebellar Purkinje cells. *Proc. Natl. Acad. Sci. USA* **92**: 8279-8282.
- DiFrancesco, D., and Noble, D. (1985) A model of cardiac electrical activity incorporating ionic pumps and concentration changes. *Phil. Trans. Roy. Soc. London Ser. B* **307**: 353-398.
- Eilers, J., Augustine, G.J., and Konnerth, A. (1995) Subthreshold synaptic  $Ca^{2+}$  signaling in fine dendrites and spines of cerebellar Purkinje neurons. *Nature* **373**: 155-158.
- Eilers, J., Plant, T., and Konnerth, A. (1996) Localized calcium signalling and neuronal integration in cerebellar Purkinje neurons. *Cell Calcium* **20**: 215-226.
- Ekerot, C.F., and Oscarsson, O. (1981) Prolonged depolarization elicited in Purkinje cell dendrites by climbing fibre impulses in the cat. *J. Physiol. (London)* **318**: 207-221.
- Fick, A. (1885) Ueber Diffusion. *Ann. Phys. Chem.* **94**: 59-86.
- Fletcher, C.A.J. (1991) *Computational Techniques for Fluid Dynamics. Volume I*. Springer-Verlag, Berlin.

- Gabbiani, F., Midtgaard, J., and Knöpfel, T. (1994) Synaptic integration in a model of cerebellar granule cells. *J. Neurophysiol.* **72**: 999-1009.
- Gamble, E., and Koch, C. (1987) The dynamics of free calcium in dendritic spines in response to repetitive synaptic input. *Science* **236**: 1311-1315.
- Garrahan, P.J., and Rega, A.F. (1990) Plasma membrane calcium pump. *Intracellular Calcium Regulation*, Bronner, F. (ed.), Alan R. Liss, New York, pp. 271-303.
- Goldbeter, A., Dupont, G., and Berridge, M.J. (1990) Minimal model for signal-induced  $Ca^{2+}$  oscillations and for their frequency encoding through protein phosphorylation. *Proc. Natl. Acad. Sci. USA* **87**: 1461-1465.
- Goldman, D.E. (1943) Potential, impedance, and rectification in membranes. *J. Gen. Physiol.* **27**: 37-60.
- Gruol, D.L., Jacquin, T., and Yool, A.J. (1991) Single-channel  $K^+$  currents recorded from the somatic and dendritic regions of cerebellar Purkinje neurons in culture. *J. Neurosci.* **11**: 1002-1015.
- Grynkiewicz, G., Poenie, M., and Tsien, R.Y.A. (1985) A new generation of  $Ca^{2+}$  indicators with greatly improved fluorescence properties. *J. Biol. Chem.* **260**: 3440-3450.
- Guyton, A.C. (1986) *Textbook of Medical Physiology*. W. B. Saunders Co., Philadelphia.
- Györke, S., and Fill, M. (1993) Ryanodine receptor adaptation: control mechanism of  $Ca^{2+}$ -induced  $Ca^{2+}$  release in heart. *Science* **260**: 807-809.
- Harvey, R.J., and Napper, R.M.A. (1991) Quantitative studies of the mammalian cerebellum. *Prog. Neurobiol.* **36**: 437-463.
- Hebb, D.O. (1949) *The Organization of Behavior: A Neuropsychological Theory*. John Wiley, New York.
- Hille, B. (1991) *Ionic Channels of Excitable Membranes*. Sinauer, Sunderland.
- Hodgkin, A.L., and Huxley, A.F. (1952) A quantitative description of membrane current and its application to conduction and excitation in nerve. *J. Physiol. (London)* **117**: 500-544.
- Hodgkin, A.L., and Katz, B. (1949) The effect of sodium ions on the electrical activity of the giant axon of the squid. *J. Physiol. (London)* **108**: 37-77.
- Hofer, A.M., and Machen, T.E. (1993) Technique for in situ measurement of calcium in intracellular inositol 1,4,5-triphosphate sensitive stores using the fluorescent indicator mag-fura-2. *Proc. Natl. Acad. Sci. USA* **90**: 2598-2602.
- Hollingworth, S., Harkins, A.B., Kurebayashi, N., Konishi, M., and Baylor, S.M. (1992) Excitation-contraction coupling in intact frog skeletal muscle fibers injected with mmolar concentrations of Fura-2. *Biophys. J.* **63**: 224-234.
- Holmes, W.R. (1995) Modeling the effect of glutamate diffusion and uptake on NMDA and non-NMDA receptor saturation. *Biophys. J.* **69**: 1734-1747.
- Holmes, W.R., and Levy, W.B. (1990) Insights into associative long-term potentiation from computational models of NMDA receptor-mediated calcium influx and intracellular calcium concentration changes. *J. Neurophysiol.* **63**: 1148-1168.

- Jack, J.J.B., Noble, D., and Tsien, R.W. (1975) *Electric Current Flow in Excitable Cells*. Clarendon Press, Oxford.
- Jaeger, D., De Schutter, E., and Bower, J.M. (1997) The role of synaptic and voltage-gated currents in the control of Purkinje cell spiking: a modeling study. *J. Neurosci.* **17**: in press.
- Jafri, M.S., and Gillo, B. (1994) A membrane potential model with counterions for cytosolic calcium oscillations. *Cell Calcium* **16**: 9-19.
- Kano, M., Garaschuk, O., Verkhratsky, A., and Konnerth, A. (1995) Ryanodine receptor-mediated intracellular calcium release in rat cerebellar Purkinje neurones. *J. Physiol. (London)* **487**: 1-16.
- Kao, J.P.Y., and Tsien, R.Y. (1988)  $Ca^{2+}$  binding kinetics of Fura-2 and azo-1 from temperature-jump relaxation measurements. *Biophys. J.* **53**: 635-1343.
- Kapicka, C.L., Carl, A., Hall, M.L., Percival, A.L., Frey, B.W., and Kenyon, J.L. (1994) Comparison of large-conductance  $Ca^{2+}$ -activated  $K^+$  channels in artificial bilayer and patch-clamp experiments. *Amer. J. Physiol.* **266**: C601-C610.
- Kargacin, G.J. (1994) Calcium signaling in restricted diffusion spaces. *Biophys. J.* **57**: 262-272.
- Kasai, H., and Petersen, O.H. (1994) Spatial dynamics of second messengers:  $IP_3$  and cAMP as long-range and associative messengers. *Trends Neurosci.* **17**: 95-101.
- Kendall, J.M., Dormer, R.L., and Campbell, A.K. (1992) Targeting aequorin to the endoplasmic reticulum of living cells. *Biochem. Biophys. Res. Comm.* **189**: 1008-1016.
- Koch, C., Poggio, T., and Torre, V. (1982) Retinal ganglion cells: a functional interpretation of dendritic morphology. *Phil. Trans. Roy. Soc. London Ser. B* **298**: 227-264.
- Koch, C., and Zador, A. (1993) The function of dendritic spines: devices subserving biochemical rather than electrical compartmentalization. *J. Neurosci.* **13**: 413-422.
- Lancaster, B., and Zucker, R.S. (1994) Photolytic manipulation of  $Ca^{2+}$  and the time, course of slow,  $Ca^{2+}$ -activated  $K^+$  current in rat hippocampal neurons. *J. Physiol. (London)* **475**: 229-239.
- Latorre, R., Oberhauser, A., Labarca, P., and Alvarez, O. (1989) Varieties of calcium-activated potassium channels. *Annu. Rev. Physiol.* **51**: 385-399.
- LeMasson, G., Marder, E., and Abbott, L.F. (1993) Activity-dependent regulation of conductances in model neurons. *Science* **259**: 1915-1917.
- Lev-Ram, V., Miyakawa, H., Lasser-Ross, N., and Ross, W.N. (1992) Calcium transients in cerebellar Purkinje neurons evoked by intracellular stimulation. *J. Neurophysiol.* **68**: 1167-1177.
- Li, Y.-X., and Rinzel, J. (1994) Equations for  $InsP_3$  receptor-mediated  $[Ca^{2+}]_i$  oscillations derived from a detailed kinetic model: a Hodgkin-Huxley like formalism. *J. Theor. Biol.* **166**: 461-473.
- Linse, S., Helmersson, A., and Forsen, S. (1991) Calcium-binding to calmodulin and its globular domains. *J. Biol. Chem.* **266**: 8050-8054.

- Llano, I., DiPolo, R., and Marty, A. (1994) Calcium-induced calcium release in cerebellar Purkinje cells. *Neuron* **12**: 663-673.
- Llano, I., Dreessen, J., Kano, M., and Konnerth, A. (1991) Intradendritic release of calcium induced by glutamate in cerebellar Purkinje cells. *Neuron* **7**: 577-583.
- Llinás, R.R., and Sugimori, M. (1980) Electrophysiological properties of in vitro Purkinje cell dendrites in mammalian cerebellar slices. *J. Physiol. (London)* **305**: 197-213.
- Llinás, R.R., Sugimori, M., and Silver, R.B. (1992) Microdomains of high calcium concentration in a presynaptic terminal. *Science* **256**: 677-679.
- Lytton, J., Westlin, M., Burk, S.E., Shull, G.E., and MacLennan, D.H. (1992) Functional comparisons between isoforms of the sarcoplasmic or endoplasmic reticulum family of calcium pumps. *J. Biol. Chem.* **267**: 14483-14489.
- Martone, M.E., Zhang, Y., Simpliciano, V.M., Carragher, B.O., and Ellisman, M.H. (1993) Three-dimensional visualization of the smooth endoplasmic reticulum in Purkinje cell dendrites. *J. Neurosci.* **13**: 4636-4646.
- Mayer, M.L., and Westbrook, G.L. (1987) Permeation and block of N-methyl-D-aspartic acid receptor channels by divalent cations in mouse cultured central neurones. *J. Physiol. (London)* **394**: 501-527.
- McCormick, D.A., and Huguenard, J.R. (1992) A model of the electrophysiological properties of thalamocortical relay neurons. *J. Neurophysiol.* **68**: 1384-1400.
- Milazzo, G. (1963) *Electrochemistry, Theoretical Principles and Practical Applications*. Elsevier, Amsterdam.
- Missiaen, L., Declerck, I., Droogmans, G., De Smedt, H., Raeymaekers, L., and Casteels, R. (1990) Agonist-dependent  $Ca^{2+}$  and  $Mn^{2+}$ -entry dependent on state of filling of  $Ca^{2+}$ -stores in aortic smooth muscle cells of the rat. *J. Physiol. (London)* **427**: 171-186.
- Miyakawa, H., Lev-Ram, V., Lasser-Ross, N., and Ross, W.N. (1992) Calcium transients evoked by climbing fiber synaptic inputs in guinea pig cerebellar Purkinje neurons. *J. Neurophysiol.* **68**: 1178-1189, 1992.
- Moczydlowski, E., and Latorre, R. (1983) Gating kinetics of  $Ca^{2+}$ -activated  $K^+$  channels from rat muscle incorporated into planar lipid bilayers. Evidence for two voltage-dependent  $Ca^{2+}$  binding reactions. *J. Gen. Physiol.* **82**: 511-542.
- Nadim, F., Olsen, Ø.H., De Schutter, E., and Calabrese, R.L. (1995) Modeling the leech heartbeat elemental oscillator. I. Interactions of intrinsic and synaptic currents. *J. Comput. Neurosci.* **2**: 215-235.
- Naraghi, M., Müller, T.H., Oheim, M., and Neher, E. (1995) Spatially resolved measurements of the endogenous calcium buffering capacity in adrenal chromaffin cells. *Abstr. Soc. Neurosci.* **21**: 1090.
- Neher, E., and Augustine, G.J. (1992) Calcium gradients and buffers in bovine chromaffin cells. *J. Physiol. (London)* **450**: 273-301.
- Nowycky, M.C., and Pinter, M.J. (1993) Time courses of calcium and calcium-bound buffers following calcium influx in a model cell. *Biophys. J.* **64**:

- 77-91.
- Olsen, Ø.H., and Calabrese, R.L. (1996) Activation of intrinsic and synaptic currents in leech heart interneurons by realistic wave-forms. *J. Neurosci.* **16**: 4958-4970.
- Palay, S.L., and Chan-Palay, V. (1974) *Cerebellar Cortex*. Springer-Verlag, New York.
- Parnas, H., Hovav, G., and Parnas, I. (1989) Effect of  $Ca^{2+}$  diffusion on the time course of neurotransmitter release. *Biophys. J.* **55**: 859-874.
- Parnas, I., Parnas, H., and Hochner, B. (1991) Amount and time course of release. The calcium hypothesis and the calcium-voltage hypothesis. *Ann. N.Y. Acad. Sci.* **635**: 177-190.
- Prakriya, M., Solaro, C.R., and Lingle, C. J. (1996)  $[Ca^{2+}]_i$  elevations detected by BK channels during  $Ca^{2+}$  influx and muscarine-mediated release of  $Ca^{2+}$  from intracellular stores in rat chromaffin cells. *J. Neurosci.* **16**: 4344-4359.
- Press, W.H., Teukolsky, S.A., Vetterling, W.T., and Flannery, B.P. (1992) *Numerical Recipes. The Art of Scientific Computing*. Cambridge University Press, Cambridge.
- Qian, N., and Sejnowski, T.J. (1989) An electro-diffusion model for computing membrane potentials and ionic concentrations in branching dendrites, spines and axons. *Biol. Cybern.* **62**: 1-15.
- Qian, N., and Sejnowski, T.J. (1990) When is an inhibitory synapse effective? *Proc. Natl. Acad. Sci. USA* **87**: 8145-8149.
- Reeves, J.P. (1990) Sodium-calcium exchange. *Intracellular Calcium Regulation*, Bronner, F. (ed.), Alan R. Liss, New York, pp. 305-347.
- Regehr, W.G., and Atluri, P.P. (1995) Calcium transients in cerebellar granule cell presynaptic terminals. *Biophys. J.* **68**: 2156-2170.
- Safri, S.M., and Keizer, J. (1995) On the roles of  $Ca^{2+}$  diffusion,  $Ca^{2+}$  buffers, and the endoplasmic reticulum in  $IP_3$ -induced  $Ca^{2+}$  waves. *Biophys. J.* **69**: 2139-2153.
- Sah, P. (1996)  $Ca^{2+}$ -activated  $K^+$  currents in neurones: types, physiological roles and modulation. *Trends Neurosci.* **19**: 150-154.
- Sala, F., and Hernandez-Cruz, A. (1990) Calcium diffusion modeling in a spherical neuron: relevance of buffering properties. *Biophys. J.* **57**: 313-324.
- Schieg, A., Gerstner, W., Ritz, R., and van Hemmen, J.L. (1995) Intracellular  $Ca^{2+}$  stores can account for the time course of LTP induction: a model of  $Ca^{2+}$  dynamics in dendritic spines. *J. Neurophysiol.* **74**: 1046-1055.
- Schoepp, D.D., and Conn, P.J. (1993) Metabotropic glutamate receptors in brain function and pathology. *Trends Pharmacol. Sci.* **14**: 13-20.
- Sherman, A., Keizer, J., and Rinzel, J. (1990) Domain model for  $Ca^{2+}$ -inactivation of  $Ca^{2+}$ -channels at low channel density. *Biophys. J.* **58**: 985-995.
- Siegel, M., Marder, E., and Abbott, L.F. (1994) Activity-dependent current distributions in model neurons. *Proc. Natl. Acad. Sci. USA* **91**: 11308-11312.

- Sneyd, J., Charles, A.C., and Sanderson, M.J. (1994) A model for the propagation of intracellular calcium waves. *Amer. J. Physiol.* **266**: C293-C302.
- Sneyd, J., Wetton, B.T.R., Charles, A.C., and Sanderson, M.J. (1995) Inter-cellular calcium waves mediated by diffusion of inositol triphosphate: a two-dimensional model. *Amer. J. Physiol.* **268**: C1537-C1545.
- Staley, K.J., Soldo, B.L., and Proctor, W.R. (1995) Ionic mechanisms of neuronal excitation by inhibitory GABA<sub>A</sub> receptors. *Science* **269**: 977-981.
- Stephenson, D.G., Wendt, I.R., and Forrest, Q.G. (1981) Non-uniform ion distribution and electrical potential in sarcoplasmic regions of skeletal muscle fiber. *Nature* **289**: 690-692.
- Takei, K., Stukenbrok, H., Metcalf, A., Mignery, G.A., Südhof, T.C., Volpe, P., and De Camilli, P. (1992)  $Ca^{2+}$  stores in Purkinje neurons: endoplasmic reticulum subcompartments demonstrated by the heterogeneous distribution of the InsP<sub>3</sub> receptor,  $Ca^{2+}$ -ATPase, and calsequestrin. *J. Neurosci.* **12**: 489-505.
- Tempia, F., Kano, M., Schneggenburger, R., Schirra, C., Garaschuk, O., Plant, T., and Konnerth, A. (1996) Fractional calcium current through AMPA-receptor channels with a low calcium permeability. *J. Neurosci.* **16**: 456-466.
- Terasaki, M., Slater, N.T., Fein, A., Schmidek, A., and Reese, T.S. (1994) Continuous network of endoplasmic reticulum in cerebellar Purkinje neurons. *Proc. Natl. Acad. Sci. USA* **91**: 7510-7514.
- Thayer, S.A., and Miller, R.J. (1990) Regulation of the intracellular free calcium concentration in single rat dorsal root ganglions *in vitro*. *J. Physiol. (London)* **425**: 85-115.
- Timmermann, M.P., and Ashley, C.C. (1986) Fura-2 diffusion and its use as an indicator of transient free calcium changes in single striated muscle cells. *Fed. Eur. Biochem. Soc. Lett.* **209**: 1-8.
- Traub, R.D., and Llinás, R. (1977) The spatial distribution of ionic conductances in normal and axotomized motoneurons. *Neurosci.* **2**: 829-850.
- Traub, R.D., Wong, R.K.S., Miles, R., and Michelson, H. (1991) A model of a CA3 hippocampal pyramidal neuron incorporating voltage-clamp data on intrinsic conductances. *J. Neurophysiol.* **66**: 635-650.
- van Egeraat, J.M., and Wikswo, J.P., Jr. (1993) A model for axonal propagation incorporating both radial and axial ionic transport. *Biophys. J.* **64**: 1287-1298.
- Wagner, J., and Keizer, J. (1994) Effects of rapid buffers on  $Ca^{2+}$  diffusion and  $Ca^{2+}$  oscillations. *Biophys. J.* **67**: 447-456.
- Wang, S.S.-H., and Augustine, G.J. (1995) Confocal imaging and local photolysis of caged compounds: dual probes of synaptic function. *Neuron* **15**: 755-760.
- Winslow, R.L., Duffy, S.N., and Charlton, M.P. (1994) Homosynaptic facilitation of transmitter release in crayfish is not affected by mobile calcium chelators: implications for the residual ionized calcium hypothesis from electrophysiological and computational analysis. *J. Neurophysiol.* **72**: 1769-1793.

- Yamada, W.M., and Zucker, R.S. (1992) Time course of transmitter release calculated from simulations of a calcium diffusion model. *Biophys. J.* **61**: 671-682.
- Zador, A., and Koch, C. (1994) Linearized models of calcium dynamics: formal equivalence to the cable equation. *J. Neurosci.* **14**: 4705-4715.
- Zador, A., Koch, C., and Brown, T.H. (1990) Biophysical model of a Hebbian synapse. *Proc. Natl. Acad. Sci. USA* **87**: 6718-6722.
- Zhou, Z., and Neher, E. (1993) Mobile and immobile calcium buffers in bovine adrenal chromaffin cells. *J. Physiol. (London)* **469**: 245-273.

Figure .8: Membrane potential (**A-B**) and  $[Ca^{2+}]$  in the submembrane shell (**C-D**) during a dendritic  $Ca^{2+}$  spike in the Purkinje cell model. Figures **B** and **D** were taken 5 msec later than **A** and **C**. In this example the dendritic spike initiated in the upper right dendrite, but this was not always the case in the model. Note that the increase in  $[Ca^{2+}]$  was delayed compared to the depolarization. The lower  $[Ca^{2+}]$  in the thick branches (the smooth dendrite) compared to the thinner branches (the spiny dendrite) was caused by the surface-to-volume ratio effect (see section 6.6.5) as the  $Ca^{2+}$  channel density was identical in all dendritic compartments.

## Legend to the Color Plate